Separation of fine and coarse aerosol modes in MFRSR data sets

Mikhail D. Alexandrov[1]
Department of Applied Physics and Applied Mathematics, Columbia University, New York, New York, USA

Barbara E. Carlson and Andrew A. Lacis
NASA Goddard Institute for Space Studies, New York, New York, USA

Brian Cairns[1]
Department of Applied Physics and Applied Mathematics, Columbia University, New York, New York, USA

Received 12 July 2004; revised 4 April 2005; accepted 12 May 2005; published 12 July 2005.

[1] A new MFRSR data analysis algorithm is presented. Our earlier algorithm assumed a monomodal aerosol size distribution, while the new algorithm allows us to partition the aerosol optical thickness into fine and coarse aerosol modes. In addition, we retrieve the fine mode effective radius and Angstrom exponent. A bimodal gamma distribution is used to describe the aerosol particle size distribution. The algorithm has been tested using a multi-year data set from the local MFRSR network at the DOE Atmospheric Radiation Measurement (ARM) Program site in Southern Great Plains (SGP). Our retrieved aerosol optical thicknesses (total, fine, and coarse) are compared with the corresponding AERONET almucantar retrieval results derived from a CIMEL sunphotometer co-located with the MFRSR at the SGP Central Facility. A constrained variant of the algorithm (zero NO_2 column values) has been used to define the range of physically justified values of the fine mode effective radius, and for comparison with AERONET particle size retrievals. We use the multiple MFRSR measurements obtained during the year 2000 at the SGP Extended Facilities to examine geographical and seasonal variability of aerosol properties. A correspondence has been found between the geographical variation in the fine mode particle size and aerosol composition (nitrates versus sulfates) as measured by National Atmospheric Deposition Program. We similarly find good correspondence between our retrieved aerosol sizes and the PM2.5 to PM10 ratios obtained from EPA AirData monitoring. Examination of the data from the SGP Central Facility obtained for the period 1993–1997 reveals a decreasing trend in coarse mode aerosol optical thickness during the 1993–1995 period, consistent with the decay of the stratospheric aerosol following the 1991 eruption of Mt. Pinatubo. In contrast, fine mode optical thickness exhibits only seasonal variability with summer maxima during this period.

Citation: Alexandrov, M. D., B. E. Carlson, A. A. Lacis, and B. Cairns (2005), Separation of fine and coarse aerosol modes in MFRSR data sets, *J. Geophys. Res.*, *110*, D13204, doi:10.1029/2004JD005226.

1. Introduction

[2] In our previous paper [*Alexandrov et al.*, 2002] we described a retrieval algorithm for Multi-Filter Rotating Shadowband Radiometer (MFRSR) data that was designed to provide a self-consistent retrieval of aerosol and gas information from the spectral dependence of the MFRSR data. In that algorithm we adopted the simplest aerosol size distribution, namely a mono-modal distribution. We showed that even for that simple, two parameter, distribution it is not possible to uniquely constrain both the effective radius and effective variance of the aerosol size distribution. In that study, we used results retrieved for size distribution variances of 0.1 and 0.4 to provide a measure of the uncertainty in the retrieved quantities. The largest source of uncertainty, as noted by *Alexandrov et al.* [2002], appears to be the spectral trade-offs between small particle aerosol extinction and NO_2 absorption. It also appears, that the assumed shape of the aerosol size distribution plays a role in these trade-offs. Comparison of spectral signatures of AOT computed with monomodal and bimodal size distributions having the same effective radius reveals qualitative differences, such that the spectral AOTs cannot be matched simply by adjusting the size

[1]Also at Nasa Goddard Institute for Space Studies, New York, New York, USA.

Copyright 2005 by the American Geophysical Union.
0148-0227/05/2004JD005226$09.00

distribution parameters. Monomodal AOT tends to have a convex spectral shape with a maximum at a wavelength near the mode's effective radius, while bimodal AOT may be concave or decrease with the wavelength. Thus, applying a monomodal aerosol model for retrievals of a bimodal aerosol may result in an overestimation of NO_2 column amounts. The NO_2–aerosol trade-offs were also analyzed by *Gianelli et al.* [2005] using the higher spectral resolution data obtained with the Rotating Shadowband Spectroradiometer (RSS) at the SGP site. The higher spectral resolution and larger spectral range of the RSS relative to the MFRSR permits better separation of aerosol and gas effects and allowed *Gianelli et al.* [2005] to conclude that the aerosol size distribution must be at least bi-modal and that the NO_2 column amounts are more consistent with lower limits provided by the large variance of *Alexandrov et al.* [2002]. Aerosol size distribution retrievals from AERONET almucantar measurements [*Dubovik et al.*, 2002] are also systematically bimodal. These concerns prompted us to investigate using a more complex aerosol size distribution and develop the analytical retrieval algorithm presented here. In our new algorithm we have adopted a bimodal aerosol size distribution consisting of a fine and coarse mode, both modeled by gamma distributions, with fine and coarse mode aerosol optical thicknesses being retrieved quantities. The effective radius of the fine mode is also retrieved, while the effective radius of the coarse mode (since it does not significantly affect the spectral variability at visible wavelengths) is held fixed at an assumed value of 1.5 μm. We use the results of Mie theory computations for a model size distribution in our inversions, rather than analytically modeling the spectral shape of aerosol extinction itself as in the study by *O'Neill et al.* [2003]. Another difference with *O'Neill et al.* [2003] is that we retrieve NO_2 column amount. Retrieval of five parameters (aerosol optical thickness (AOT) of the fine mode, AOT of the coarse mode, effective radius of the fine mode, ozone and NO_2 column amounts) is a difficult practical task considering the uncertainties in the instrument calibration (that we determine from the data) and other minor technical imperfections affecting the data quality, such as instrument tilts, errors in the lab-measured angular response function, and signal noise. To deal with these problems we use some regularization techniques, such as noise filtering (with Wiener filter assuming a power-law model spectrum), as well as suppressing the variability of the fine mode radius during the day. Nitrogen dioxide through the spectral trade-offs between its column amount and size of fine mode aerosols remains a major source of uncertainty in aerosol size retrievals. To investigate the influence of NO_2 on our results we developed a constrained variant of our algorithm allowing for retrievals of aerosol properties and ozone column while assuming a fixed column amount (including zero) of NO_2. The results obtained with the constrained method assuming zero NO_2 correspond to the smallest physically justified values of the fine mode effective radius. In this paper, in addition to the method description, we present intercomparisons of our results with AERONET almucantar retrievals [*Dubovik and King*, 2000], as well as a qualitative testing of how well our retrievals capture known aerosol events (Pinatubo volcanic aerosols) and ambient properties (geographic variations in aerosol size and composition across the SGP site from northern Kansas to south-eastern Oklahoma).

2. Method

2.1. MFRSR Measurements

[3] The MFRSR makes precise simultaneous measurements of the direct solar beam extinction and horizontal diffuse flux, at six wavelengths (nominally 415, 500, 615, 670, 870, and 940 nm) at short (20 sec in our data set) intervals throughout the day. Besides water vapor at 940 nm, the other gaseous absorbers within the MFRSR channels are NO_2 (at 415, 500, and 615 nm) and O_3 (at 500, 615, and 670 nm). Aerosols and Rayleigh scattering contribute atmospheric extinction in all MFRSR channels.

[4] Using the notation of *Alexandrov et al.* [2002] for the inversion problem description, we represent the direct solar beam irradiance $I^{(i)}$ measured by the MFRSR at each time step in the ith spectral channel in the form:

$$I^{(i)} = C^{(i)} I_0^{(i)} \exp\left(-\frac{\tau^{(i)}}{\mu}\right), \tag{1}$$

where μ is the inverse of the airmass (essentially equal to the cosine of the solar zenith angle for small to moderate values of the latter), $\tau^{(i)}$ is the atmospheric column extinction optical depth corresponding to the ith channel and $I_0^{(i)}$ are the TOA nominal solar intensities. As the notation implies, we take the lamp calibrated intensities and determine the correction factors $C^{(i)}$ to the original (lamp) calibration which is used only for a rough conversion of counts to Wm^{-2}. The directly computed optical thicknesses $\tilde{\tau}^{(i)}$ in the ith spectral channel can then be written as

$$\tilde{\tau}^{(i)} = -\ln\left(\frac{I^{(i)}}{I_0^{(i)}}\right) \cdot \mu = \tau^{(i)} + c^{(i)}\mu, \tag{2}$$

where $c^{(i)} = -\ln C^{(i)}$ is the calibration coefficient which is equal to zero in the absence of lamp calibration errors.

[5] An automatic cloud screening procedure [*Alexandrov et al.*, 2004a] is used to select clear-sky intervals throughout the day. Our algorithm is applied simultaneously to sets of daily MFRSR records spanning at least one month of measurements. The data processing is iterative in nature and runs by subsequently increasing the "data level" of the whole data set: first all days are cloud screened, then all 870 nm records are calibrated using compatibility between the direct and diffuse measurements, etc. This approach facilitates the stabilization of the daily calibration constants at each level using a robust smoothing of the month(s)-long calibration record.

2.2. Aerosol Size Distribution Information Content in MFRSR Measurements

[6] We begin our analysis by removing from the MFRSR measurements the Rayleigh scattering contribution following *Hansen and Travis* [1974]. Then, the system expressing the measured $\tilde{\tau}_i$ in terms of the parameters to be retrieved takes the form:

$$\tilde{\tau}^{(1)} = q^{(1)}\tau_a^{(5)} + \beta^{(1)} x_{NO_2} + c^{(1)}\mu \tag{3}$$

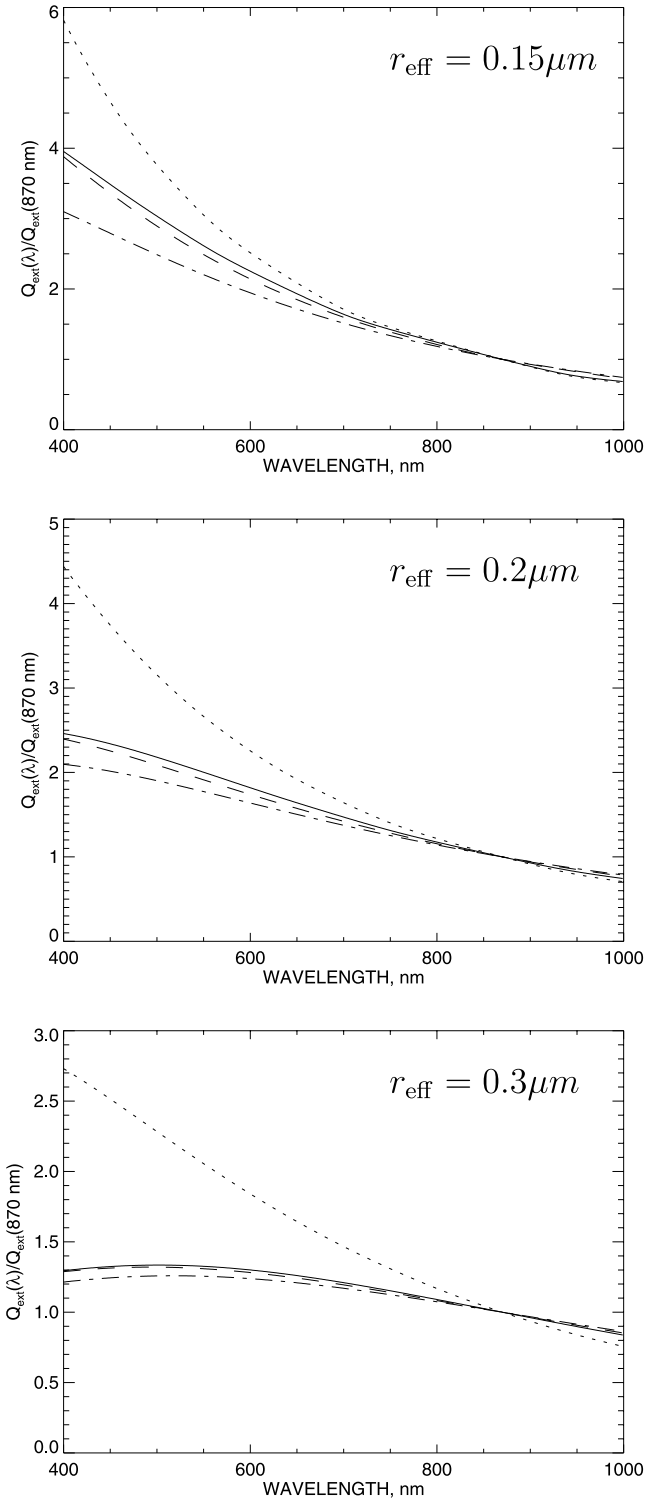

Figure 1. Sensitivity of the aerosol extinction spectral shape to the real part of the refractive index n_r for three model cases with aerosol effective radius r_{eff} = 0.15, 0.2, and 0.3 μm. Dotted and solid curves depict the normalized spectral extinction $Q_{\text{ext}}(\lambda)/Q_{\text{ext}}(870\ \text{nm})$ respectively for n_r = 1.6 and n_r = 1.33. The aerosol models with n_r = 1.33 and r_{eff} rescaled using the standard (15) and modified (16) formulas are represented by the dot-dashed and dashed curves, respectively.

$$\tilde{\tau}^{(2)} = q^{(2)}\tau_a^{(5)} + \beta^{(2)}x_{NO_2} + \gamma^{(2)}x_{O_3} + c^{(2)}\mu \quad (4)$$

$$\tilde{\tau}^{(3)} = q^{(3)}\tau_a^{(5)} + \beta^{(3)}x_{NO_2} + \gamma^{(3)}x_{O_3} + c^{(3)}\mu \quad (5)$$

$$\tilde{\tau}^{(4)} = q^{(4)}\tau_a^{(5)} + \beta^{(4)}x_{NO_2} + \gamma^{(4)}x_{O_3} + c^{(4)}\mu \quad (6)$$

$$\tilde{\tau}^{(5)} = \tau_a^{(5)} + c^{(5)}\mu. \quad (7)$$

Here $q^{(i)} = Q_{\text{ext}}^{(i)}/Q_{\text{ext}}^{(5)}$, where $Q_{\text{ext}}^{(i)}$ is the aerosol extinction ratio which can be computed using Mie theory. Obviously, $q^{(5)} = 1$. $\beta^{(i)}$ and $\gamma^{(i)}$ are the effective spectral absorption coefficients for NO_2 and O_3, respectively, weighted by the solar flux and filter response function of each respective MFRSR channel (the coefficients $\beta^{(5)}$, $\gamma^{(1)}$ and $\gamma^{(5)}$ are effectively equal to zero); x_{NO_2} and x_{O_3} are respective column amounts of NO_2 and ozone; $\tau_a^{(5)}$ is the aerosol optical thickness in MFRSR channel 5 (at 870 nm).

[7] The calibration constant $c^{(5)}$ is determined from a consistency condition between AOTs derived from the direct beam and from calibration-independent direct-to-diffuse ratios. After this operation, $\tau_a^{(5)} = \tilde{\tau}^{(5)} - c^{(5)}\mu$ becomes a known quantity. In the above set of equations the explicit dependence on x_{NO_2} and x_{O_3} can be eliminated by simple row reduction leading to the following two equations:

$$G^{(3)} = B^{(3)} + A^{(3)}y \quad (8)$$

$$G^{(4)} = B^{(4)} + A^{(4)}y, \quad (9)$$

where

$$y = \frac{\mu}{\tau_a^{(5)}} \quad (10)$$

$$G^{(i)} = \Xi^{(i)}(\tilde{\tau})/\tau_a^{(5)} \quad (11)$$

$$B^{(i)} = \Xi^{(i)}(q) \quad (12)$$

$$A^{(i)} = \Xi^{(i)}(c), \quad (13)$$

i = 3, 4. We used the linear functional

$$\Xi^{(i)}(f) = f^{(i)} - \frac{\beta^{(i)}}{\beta^{(1)}}f^{(1)} - \frac{\gamma^{(i)}}{\gamma^{(2)}}\left(f^{(2)} - \frac{\beta^{(2)}}{\beta^{(1)}}f^{(1)}\right) \quad (14)$$

of a vector $f = [f^{(1)}, f^{(2)}, f^{(3)}, f^{(4)}]$ to simplify the expressions here and throughout the paper. Time series of $B^{(3)}$ and $B^{(4)}$ are obtained from (8) and (9) after the calibration constants $A^{(3)}$ and $A^{(4)}$ are determined by regressions in y (slower variability of $B^{(i)}$ compared to y is assumed). The parameters $B^{(3)}$ and $B^{(4)}$ contain all of the retrievable aerosol size distribution information.

2.3. Aerosol Size Distribution Model

[8] We assume that the aerosol size distribution has a bimodal form, and adopt a gamma distribution with fixed

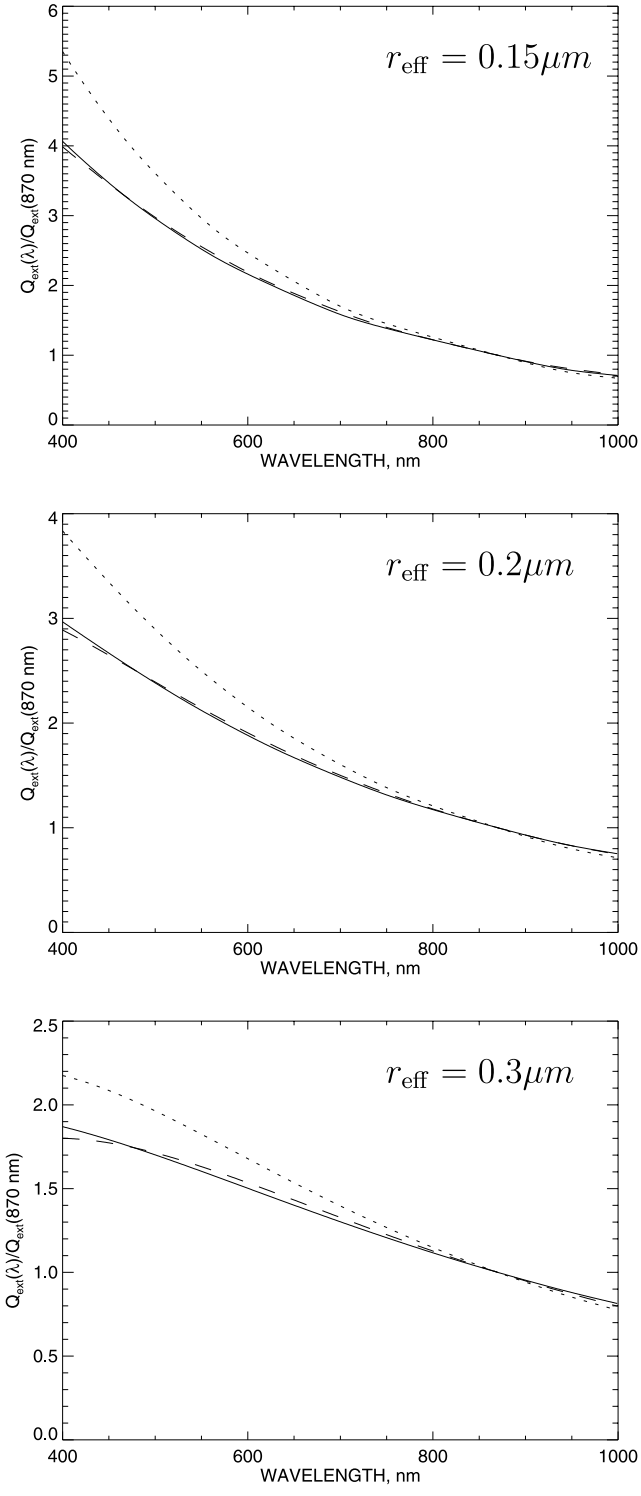

Figure 2. Sensitivity of the aerosol extinction spectral shape to the effective variance of the size distribution for three model cases with aerosol effective radius r_{eff} = 0.15, 0.2, and 0.3 μm. Solid and dotted curves depict the normalized spectral extinction $Q_{\text{ext}}(\lambda)/Q_{\text{ext}}(870\ \text{nm})$ respectively for $v_{\text{eff}} = 0.4$ and $v_{\text{eff}} = 0.2$. The gamma distribution is used as the analytical model for the aerosol size distribution. The real part of the refractive index is assumed to be n_r = 1.4. The dashed curve represents the aerosol model with $v_{\text{eff}} = 0.2$ and the effective radius rescaled (divided in each case by respectively 0.77, 0.81, and 0.88).

effective variance $v_{\text{eff}} = 0.2$ as a reasonable value for both modes (see *Hansen and Travis* [1974] for definitions of gamma distribution, effective radius, and variance). The coarse mode is assumed to have a fixed effective radius r_{eff} = 1.5 μm, while the fine mode radius is a retrieved quantity. For simplicity, the aerosol is assumed to be non-absorbing with the real part of the refractive index equal to n_r = 1.4 for both modes.

[9] Sensitivity of retrieved aerosol sizes to the assumed value of the aerosol refractive index is given approximately via the anomalous diffraction approximation [cf. *van de Hulst*, 1981; *Franssens et al.*, 2000] whereby the extinction efficiency of the aerosol is shown to depend on particle size and refractive index in the form $a(n_r - 1)$, where a is a characteristic size (e.g., r_{eff}). This means that for a given assumed refractive index n_r and the actual value $n_r^{(true)}$ the retrieved r_{eff} is related to the true effective radius by

$$r_{\text{eff}} = \frac{n_r^{(true)} - 1}{n_r - 1} \cdot r_{\text{eff}}^{(true)}. \tag{15}$$

We can quantify this further using Mie scattering results for the aerosol spectral extinction across the visible spectral range and by introducing a correction factor ζ such that

$$r_{\text{eff}} = \frac{n_r^{(true)} - 1}{n_r - 1} \cdot \frac{r_{\text{eff}}^{(true)}}{\zeta}, \tag{16}$$

where ζ depends on $r_{\text{eff}}^{(true)}$, $n_r^{(true)}$, and n_r. To illustrate this relation, we present in Figure 1 the spectral extinction curves for extreme values of refractive index $n_r^{(true)}$ = 1.6 (solid line) and n_r = 1.33 (dotted line) with gamma size distributions having v_{eff} = 0.2 and $r_{\text{eff}}^{(true)}$ = 0.15, 0.2, and 0.3 μm, for which the corresponding values of ζ are 1.2, 1.1, and 1.05 respectively. The curves of aerosol spectral extinction are normalized to unity at 870 nm, and are equivalent to spectral AOT having the value of 1 at this wavelength. Taking equation (15) for r_{eff}, we obtain the dot-dashed curve for spectral extinction, while equation (16) (dashed line) gives an even closer fit to the solid line. These comparisons demonstrate that for the limited spectral range sampled by MFRSR, the retrieved quantity is effectively the product of the aerosol size and refractive index so that errors in assumed aerosol n_r are compensated by corresponding changes in aerosol effective radius such that the spectral AOT (at visible wavelengths) remains unaffected within the accuracy of the measurements (estimated as 0.01 in AOT for typical values of 0.1–0.2 at 550 nm wavelength). Thus, potential errors in the assumed value of n_r do not affect the separation of aerosol modes or the retrievals of ozone and NO_2, which are based on spectral characteristics of the components. A possible difference in refractive indices between the two modes is also not important for our retrievals, since the coarse mode n_r, as well as the coarse effective radius (assumed to be fixed), has only a weak effect on aerosol extinction at visible wavelengths.

[10] Similarly, should the effective variance of the fine mode differ from our assumed value (v_{eff} = 0.2) we need only rescale the retrieved effective radius according to

$$r_{\text{eff}} = \frac{r_{\text{eff}}^{(true)}}{\delta}. \tag{17}$$

In equation (17), $r_{\text{eff}}^{(true)}$ is the effective radius of the actual aerosol size distribution with effective variance $v_{\text{eff}}^{(true)}$, and r_{eff} is the effective radius of the assumed distribution with effective variance v_{eff}. The rescaling factor δ depends on all of these quantities. As in Figure 1, Figure 2 shows the spectral dependence of the aerosol extinction, normalized to unity at 870 nm. For this comparison we used $n_r = 1.4$, $v_{\text{eff}}^{(true)} = 0.4$ and $v_{\text{eff}} = 0.2$ for the gamma distribution, and considered three representative cases with $r_{\text{eff}}^{(true)} = 0.15$, 0.2, and 0.3 μm. As can be seen, rescaling according to (17) using $\delta = 0.77$, 0.81, and 0.88, respectively, leads to spectral extinctions that are indistinguishable, within the measurement accuracy, from the true values. These sensitivity studies confirm the findings of our earlier paper [*Alexandrov et al.*, 2002] that retrievals based on sparsely sampled spectral measurements at visible wavelengths lead to a well-constrained family of aerosol size distributions that fit the measurement data, rather than a unique solution. Since there is little spectral sensitivity to the coarse mode aerosol properties in the visible range the particular value of the coarse mode effective variance is not important.

2.4. Separation Between Fine and Coarse Aerosol Modes

[11] It should be emphasized that variations in aerosol fine mode size and in the partition between fine and coarse modes have a similar effect on the spectral signature of AOT, and this complicates determination of aerosol size parameters. In the procedure described below we follow the general approach of section 2.2. First, an analytical combination of measured parameters is constructed, which depends only on the fine mode r_{eff}. After the r_{eff} is retrieved from this combination, the fraction of fine mode in total AOT can be also determined.

[12] We parameterize the fine mode r_{eff} as

$$r_{\text{eff}} = \eta \cdot r_{\text{eff}}^{(\min)}, \tag{18}$$

where $r_{\text{eff}}^{(\min)} = 0.2$ is the minimum value of r_{eff} for which the overlapping NO_2 absorption is not an issue, and where $\eta \geq 1$ is a scaling factor. In the context of hygroscopic particle growth, $r_{\text{eff}}^{(\min)}$ and η can be regarded as the dry aerosol size and the hygroscopic growth factor, respectively [cf. *Li et al.*, 2001]. As described below, the value 0.2 has been optimally selected for $r_{\text{eff}}^{(\min)}$ in order to avoid the uniqueness issues that arise for small η when the spectral slope of aerosol extinction begins to resemble that of NO_2 absorption.

[13] Total AOT can be expressed as the sum of the optical thicknesses of fine (τ_f) and coarse (τ_c) modes:

$$\tau_a = \tau_f + \tau_c. \tag{19}$$

Using bi-modal parameters analogous to those employed in equations (3)–(7), we introduce fine and coarse extinction ratios $q_f(\eta)$ and q_c such that

$$\tau_c^{(i)} = q_c^{(i)} \cdot \tau_c^{(5)}, \quad \tau_f^{(i)}(\eta) = q_f^{(i)}(\eta) \cdot \tau_f^{(5)}. \tag{20}$$

[14] Taking into account (19), linearity of Ξ allows for decomposition of $B^{(i)} \cdot \tau_a^{(5)}$ into a sum of fine and coarse mode contributions:

$$B^{(i)} \cdot \tau_a^{(5)} = \Xi^{(i)}(\tau_a) = P_f^{(i)}(\eta) \cdot \tau_f^{(5)} + P_c^{(i)} \cdot \tau_c^{(5)} \tag{21}$$

with

$$P_f^{(i)}(\eta) = \Xi^{(i)}\big(q_f(\eta)\big), \quad P_c^{(i)} = \Xi^{(i)}(q_c). \tag{22}$$

Dividing both parts of this equation by $\tau_a^{(5)}$ and using (19) we obtain

$$B^{(i)} - P_c^{(i)} = \left(P_f^{(i)}(\eta) - P_c^{(i)}\right) \cdot \nu_f^{(5)} \tag{23}$$

where

$$\nu_f^{(5)} = \frac{\tau_f^{(5)}}{\tau_a^{(5)}} \tag{24}$$

is the fraction of the fine mode in 870 nm AOT. Equation (23) can be written in the form

$$B^{(i)} = \nu_f^{(5)} P_f^{(i)}(\eta) + \left(1 - \nu_f^{(5)}\right) P_c^{(i)}, \tag{25}$$

that reveals the symmetry under the transformation $\nu_f \leftrightarrow (1 - \nu_f)$ and the two degenerate cases ($\nu_f = 0$ and $\nu_f = 1$), when only one of the modes is present.

[15] The combination of equation (23) for $i = 3, 4$ leads to the non-linear equation for η (or equivalently for the fine mode effective radius):

$$S(\eta) = B_s. \tag{26}$$

Here

$$S(\eta) = \frac{P_f^{(4)}(\eta) - P_c^{(4)}}{P_f^{(3)}(\eta) - P_c^{(3)}}, \tag{27}$$

$$B_s = \frac{B^{(4)} - P_c^{(4)}}{B^{(3)} - P_c^{(3)}}. \tag{28}$$

$S(\eta)$, computed using Mie theory, is a monotonically decreasing function of η (see Figure 3) provided that $r_{\text{eff}}^{(\min)} \geq 0.13$ (i.e. $r_{\text{eff}} \geq 0.13$ for all η), otherwise oscillations start to occur at small η making solution of (26) non-unique. As shown in Figure 3, the value of S has little sensitivity to the effective radius in the interval $0.2 \geq r_{\text{eff}} \geq 0.13$. This effect, which is due to similarity in spectral slope between small particle extinction and NO_2 absorption, makes retrievals in this size range ambiguous and results in excessive variability of the retrieved r_{eff}, and fine and coarse mode AOTs. Note, that constraining the retrievals by assuming a fixed NO_2 column amount (e.g. zero) eliminates this ambiguity. Because of these spectral trade-offs between aerosol extinction and NO_2 absorption, we set $r_{\text{eff}}^{(\min)} = 0.2$ μm, as the smallest aerosol effective radius that we can

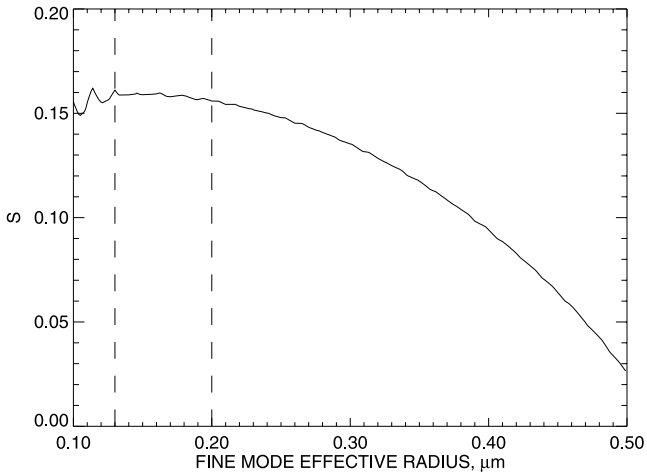

Figure 3. Plot of the function S defined by equation (27) versus the aerosol fine mode effective radius. The dashed lines correspond to $r_{\text{eff}} = 0.13$ and 0.2 μm.

reliably retrieve when simultaneously retrieving the NO_2 column amount. The cases for which the data suggests r_{eff} smaller than 0.2 μm are analyzed separately using a default value of the effective radius (equal to $r_{\text{eff}}^{(\min)}$ in our algorithm). Also, in order to better constrain the aerosol effective radius in these cases we perform constrained retrievals with the NO_2 column amount set to zero. This has the effect of adding any existing extinction of atmospheric NO_2 to that of the aerosol. Given the spectral signature of NO_2, this operation increases the aerosol spectral extinction slope and leads to a smaller value of the retrieved fine mode radius, as is shown by the grey curves in Figure 4. Thus, these constrained retrievals with NO_2 set to its minimum value provide a lower limit to the aerosol fine mode effective radius. We should repeat, that in the size range of $r_{\text{eff}} < 0.2$ μm, NO_2 absorption cannot be fully separated from aerosol extinction based on the limited spectral sampling of MFRSR measurements, thus the size values in this range obtained with constrained and unconstrained NO_2 should be considered as the bounds of the solution space that contains the actual fine mode aerosol size.

[16] The $B^{(3)}$ and $B^{(4)}$ entering formula (28) for B_s are obtained from equations (8) and (9), and are determined by the instrument data. Mie theory is used to compute $P_c^{(i)}$. The parameter B_s depends on small spectral differences in the measurements, and, therefore, is sensitive to both instrumental noise and systematic errors (discrepancies in angular response due to filter degradation or instrument tilt). To deal with the noise, we apply the Wiener filter assuming a power-law shape of the AOT time series frequency spectrum (see *Alexandrov et al.* [2004b] for variability analysis of AOT time series). To reduce the influence of (low-frequency) systematic errors, we reduce the total variation of $B_s(t)$ by a factor of 10:

$$B_s(t) \to \overline{B_s} + \frac{1}{10}\left(B_s(t) - \overline{B_s}\right) = 0.9 \cdot \overline{B_s} + 0.1 \cdot B_s(t), \qquad (29)$$

here $\overline{B_s}$ is the daily mean of B_s. This suppresses rapidly changing and anti-correlated (unphysical) fine and coarse AOTs retrieved from the slowly changing total AOT.

[17] If $B_s > S(1)$ a numerical solution for η cannot be found. This situation is an indication of very small fine mode size. If encountered, we set $\eta = 1$, which implies the default value of $r_{\text{eff}}^{(\min)}$. However in this case setting the default value of r_{eff} to $r_{\text{eff}}^{(\min)}$ defines the upper boundary for the possible effective radius.

[18] When η is well determined, the value of $\nu_f^{(5)}$ is found from (23). In some cases one of the modes may be absent ($\nu_f^{(5)} = 0$ or 1) and the size distribution becomes monomodal. Another case of effective mono-modality occurs when fine mode particles are sufficiently large so as to make the distinction between the two modes unreliable given the limited spectral sampling and range of MFRSR measurements. This may then lead to unphysical solutions with $\nu_f^{(5)} < 0$ or $\nu_f^{(5)} > 1$. Indeed, in the extreme hypothetical case when the fine mode grows to the size of the coarse mode, separation between them becomes impossible and $\nu_f^{(5)}$ can become an arbitrary number (formally even negative). In these cases when $\nu_f^{(5)}$ appears to be outside the unit interval, and also when the retrieved fine mode $r_{\text{eff}} > 0.5$ μm, we assume the aerosol to be effectively monomodal and repeat the inversion using a monomodal aerosol size distribution model (gamma distribution with retrievable r_{eff}, same as used for the fine mode). The restrictions (29) on variability of B_i are not applied for monomodal retrievals. For monomodal aerosol size distribution η can be found from the simple equation

$$B^{(i)} = P_m^{(i)}(\eta), \qquad (30)$$

for $i = 3$ ($i = 4$ can be used as well), where we adopt $P_m^{(i)} = P_f^{(i)}$. Retrievals for large r_{eff} are unreliable due to the spectral flatness of the Mie-derived extinction curves and the limited spectral range of the MFRSR data. Thus, if the retrieved monomodal $r_{\text{eff}} > 1.5$ μm, we set it equal to the default coarse mode size. In general, attributing the monomodal AOT to either the fine or coarse mode is made with respect to the retrieved particle size and fine or coarse AOT continuity for given day (if available).

3. Applications and Intercomparisons

[19] In this section we describe the results of our separation method applied to the MFRSR data set from the local network at the U.S. Southern Great Plains (SGP) run by the DOE Atmospheric Measurement (ARM) Program (Figure 5). The network consists of 21 instruments located at SGP's Extended Facilities (EFs) and covers the area of approximately 3 by 4 degrees in northern Oklahoma and southern Kansas with average spacing of 80 km between neighboring measurement sites. To ensure that noise filtering and other regularization techniques are properly applied to the MFRSR data, we performed some quantitative and qualitative comparisons of our retrievals with other aerosol measurements made at SGP's Central and Extended Facilities.

3.1. Comparison With AERONET Almucantar Scan Retrievals

[20] We compared our results with the total, fine, and coarse AOTs obtained from AERONET almucantar retrievals [*Dubovik and King*, 2000] for 870, 670, and 440 nm

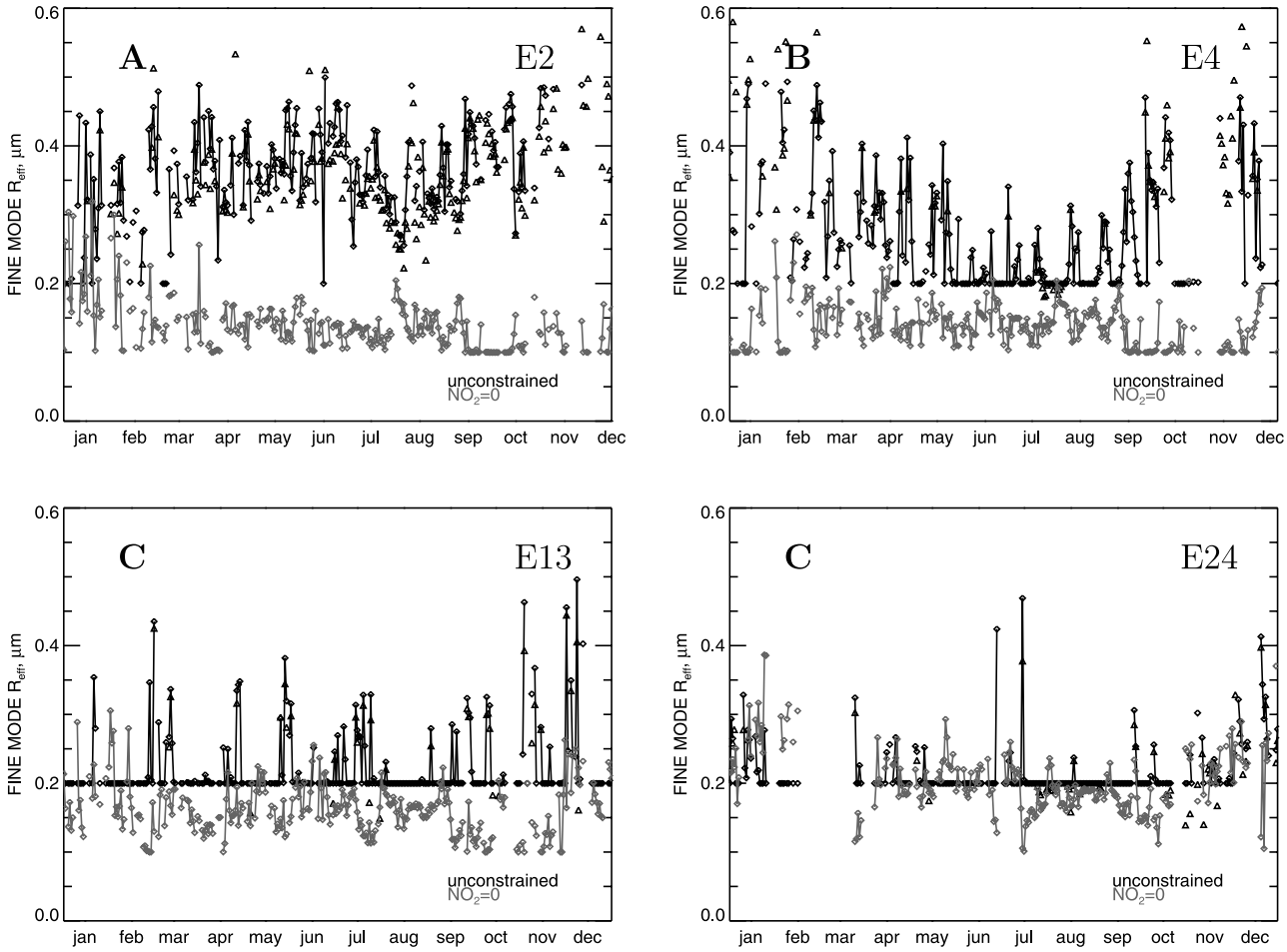

Figure 4. Time series of daily mean fine mode effective particle radius for SGP Extended Facilities E2, E4, E13, and E24 (see Figure 5) for the year 2000. These illustrate the three characteristic types of variability: A, NE and SW of the site, large 0.3–0.4 μm particles with no annual cycle; B, NW and center, intermediate type with larger particles in winter; C, center and SE, mostly very small fine mode particles (smaller than or equal to the retrieval threshold of 0.2 μm). E13 can be attributed to both types B and C. Black curves represent values obtained without any constraints on NO_2 column amounts. Diamonds correspond to retrieved effective radii of bimodal distribution, and triangles represent the cases when mode separation was not possible and show r_{eff} of the monomodal distributions used. Grey curves show the retrievals with zero NO_2 condition imposed. They provide the lower bound for possible values of fine r_{eff}. The plots reveal larger difference between the constrained and unconstrained retrievals for E2 and E4 located in northern Kansas close to large pollution sources compared to relatively clean E13 and especially E24 sites.

CIMEL sun-photometer channels (the 440 nm results were compared with optical thickness interpolated from MFRSR 415 and 500 nm channels). Since the NO_2 contribution is not separated from AOT in the AERONET data set, the NO_2 optical thicknesses retrieved from MFRSR measurements were added to total and fine mode AOT at 440 and 670 nm before comparison. We used the data from the CIMEL sunphotometer labeled ''Cart Site'' on the AERONET web site, which is colocated with the two SGP's Central Facility MFRSRs (C1 and E13, see Figure 5 for the instruments locations). For a clear day, up to 4 AERONET almucantar scan retrievals are available. These retrievals are based on the analysis of both spectral and angular dependences of the scattered radiation. The inclusion of sky-radiation measurements in the analysis can potentially help to constrain aerosol properties (coarse mode in particular), however it introduces additional uncertainties associated with the multiple scattering calculations, namely dependence on surface albedo and aerosol particle shape. The latter problem was addressed by *Dubovik et al.* [2002] who reported an artificial increase in retrieved concentrations of particles smaller than 0.1 μm in the presence of nonspherical coarse mode aerosols. Thus, not accounting for particle nonsphericity would result in an underestimation of fine mode effective radius. Direct-sun measurements, on the other hand, are not sensitive to particle shape.

[21] The Angstrom exponent is frequently used as a measure of aerosol size since it is largely independent of retrieval model assumptions. Figure 6 shows a comparison between the 440–870 nm Angstrom exponents obtained

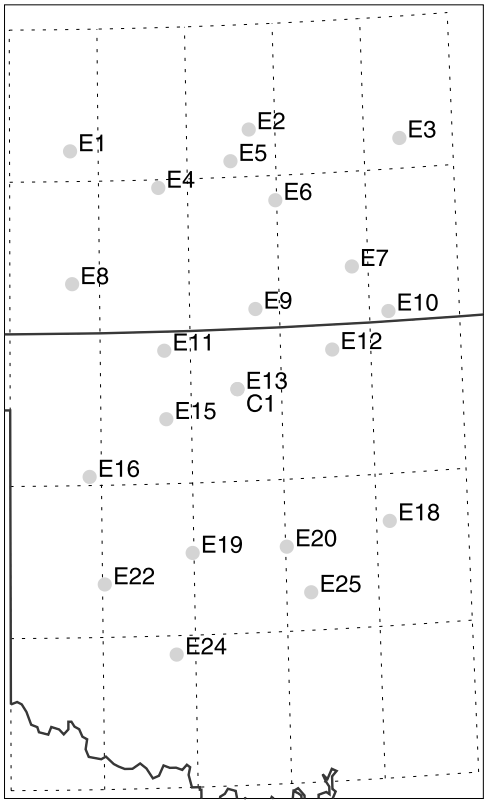

Figure 5. Locations of MFRSRs at the DOE ARM program CART site in the Southern Great Plains (SGP). The location of the Extended Facility E13 coincides with the Central Facility C1.

from all AERONET almucantar retrievals in 2000 and those calculated from corresponding MFRSR retrievals (the latter were computed using calibrated total optical thickness with the ozone contribution subtracted). The MFRSR values are taken from the measurements closest in time to the almucantar scans and fall within 5 minutes of them. On average the differences between MFRSR and AERONET Angstrom exponents are of the same order as those between the values from almucantar and the ordinary spectral extinction AERONET measurements (middle left plot in Figure 6), however the latter two may be up to 10 minutes apart. The largest differences are related to smaller AOT (bottom plots in Figure 6), and to the less well determined MFRSR calibrations in winter due to fewer clear days. The agreement between Angstrom exponents computed from the two MFRSRs (C1 and E13) data is better than between each MFRSR and AERONET (Figure 6, middle right plot), since the same calibration technique has been applied to both MFRSR data sets. While MFRSR spectral measurements are simultaneous in time, CIMEL makes almucantar scans in different spectral channels sequentially, and this separation in time may allow temporal fluctuations in AOT to produce noise in the Angstrom exponents in AERONET almucantar data. The remaining differences between the two MFRSRs (Figure 6, middle right plot) can be attributed mostly to sampling errors in calibration, since intervals of missing data are different for the two instruments. Both low AOT and calibration effects are expected to affect our aerosol size retrievals. However, as shown below, the primary difference between our aerosol sizes and those determined by AERONET arise from the different treatment of NO_2 absorption: while we retrieve an NO_2 column the AERONET retrievals neglect this gas.

[22] The results of the comparison between AOT at 870 nm for the period from March 1998 to September 2000 (576 datapoints) are presented in Figure 7. The plots show that while agreeing on average in total AOT, our retrievals have a small positive bias of 0.01 (or 10%) on average for fine mode AOT compared with the AERONET values (and a corresponding negative bias for coarse mode AOT). Comparisons of the optical thicknesses in the 670 and 440 nm CIMEL channels yield similar results. As we have shown above, the spectral dependence of AOT in our retrievals is not affected by assumptions regarding the real part of the aerosol refractive index or the v_{eff} of the aerosol size distribution. However, the value of the fine mode r_{eff} has an effect on the mode separation biases. To illustrate this we compared our retrievals with the results of a constrained (zero NO_2) run, that produces smaller r_{eff} values similar to those of AERONET (see below) on a shorter test data set June–September, 2000 from E13. The results obtained with our standard retrieval assumptions are similar to those in Figure 7: biases of MFRSR over AERONET were 0.009 in total, 0.015 in fine, and −0.007 in coarse AOT, while application of the constrained (zero NO_2) algorithm showed much better agreement with AERONET: 0.009 in total, 0.0045 in fine, and 0.0044 in coarse AOT. This indicates, that the larger (0.015) positive bias in fine mode AOT for unconstrained (NO_2 retrieved) comparison relative to the smaller (0.0045) bias in the constrained (zero NO_2) case is a consequence of the larger particle size that we retrieve by accounting for the spectral contribution of NO_2 absorption. The remaining small positive biases in both fine and coarse AOTs contain contributions from differences in instruments calibrations and

Figure 6. (top) Comparison between MFRSR-derived 440–870 nm Angstrom exponents with those from AERONET almucantar scan analysis. The data sets from the SGP site Central Facility MFRSRs (C1,E13) and CIMEL for the year 2000 has been used. The MFRSR 440 nm optical thickness values are obtained by linear interpolation between total measured optical depths in 415 and 500 nm channels with ozone contribution subtracted. (middle) Comparison between AERONET's Angstrom exponents obtained from almucantar retrievals and these from the closest regular spectral measurements (left), and comparison between exponents from the two MFRSR data sets (C1, E13) sampled at the time points used in the top plots (right). (bottom) The differences in the values of Angstrom exponents between E13 MFRSR and AERONET almucantar data sets (left) and between two MFRSR data sets (right) as function of AOT. The maximal errors appear to be proportional to the inverse AOT values (dashed curves). In addition to small AOT possible uncertainties in MFRSR calibrations in winter (when number of clear days is small) can contribute to the differences.

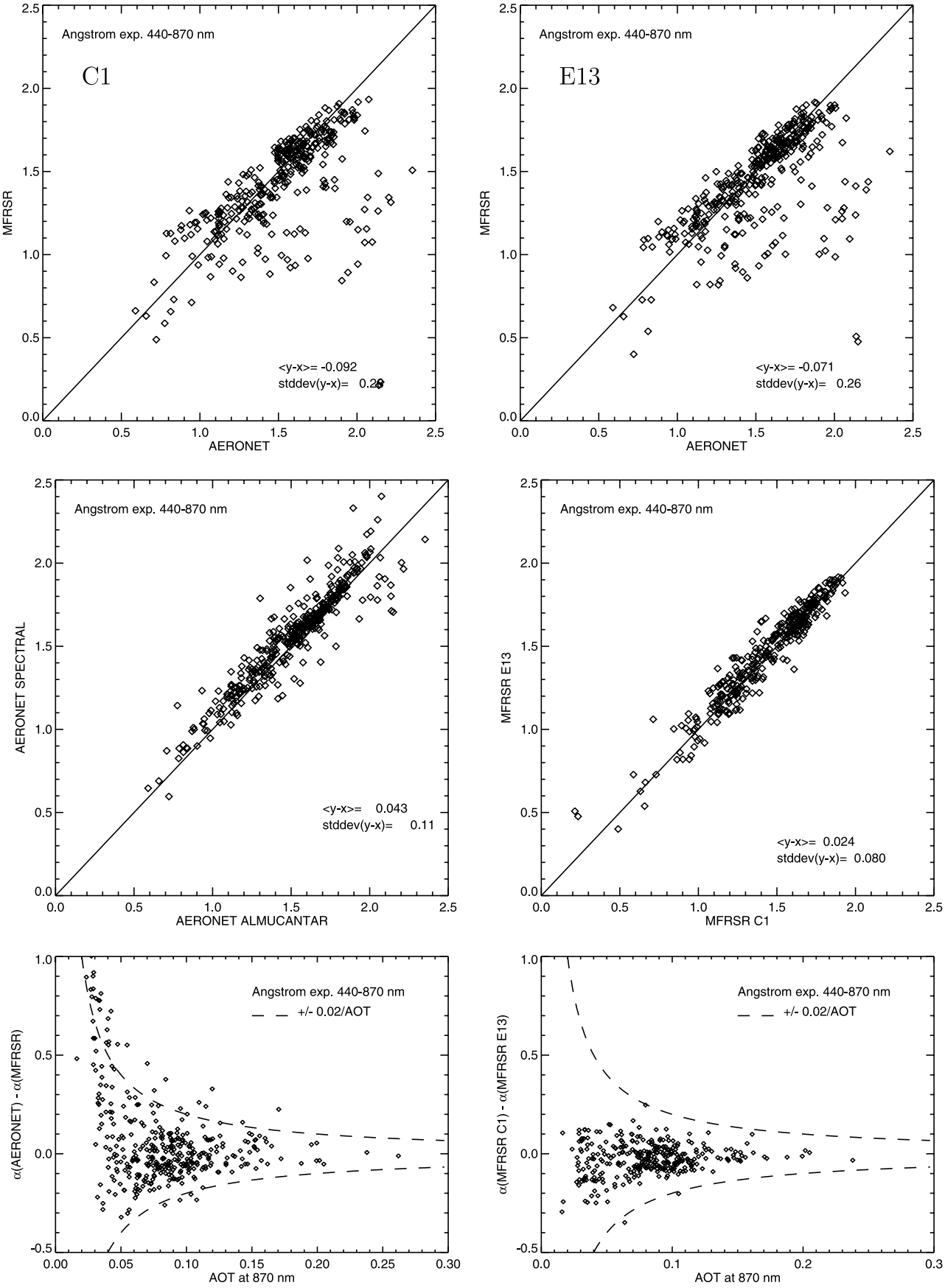
Angstrom exp. 440-870 nm
C1
MFRSR
AERONET
<y-x>= -0.092
stddev(y-x)= 0.26
Angstrom exp. 440-870 nm
E13
MFRSR
AERONET
<y-x>= -0.071
stddev(y-x)= 0.26
Angstrom exp. 440-870 nm
AERONET SPECTRAL
AERONET ALMUCANTAR
<y-x>= 0.043
stddev(y-x)= 0.11
Angstrom exp. 440-870 nm
MFRSR E13
MFRSR C1
<y-x>= 0.024
stddev(y-x)= 0.080
Angstrom exp. 440-870 nm
+/- 0.02/AOT
α(AERONET) - α(MFRSR)
AOT at 870 nm
Angstrom exp. 440-870 nm
+/- 0.02/AOT
α(MFRSR C1) - α(MFRSR E13)
AOT at 870 nm

Figure 6

uncertainties in aerosol model assumptions (e.g. shape of aerosol size distribution, particle non-sphericity).

[23] The fine mode effective radius in AERONET retrievals for the period of the comparison presented in Figure 7 and for 2000 (Figure 4, left bottom panel) were always lower than our effective retrieval limit of 0.2 μm, thus they are not suitable for a quantitative comparison. Domination of small ($\leq$0.2 μm) particles at the SGP Central Facility is in qualitative agreement with our results for the year 2000, however we also detect a number of days when the aerosols were notably larger. However, our retrievals made under zero NO_2 assumption (grey curve in Figure 7), same as used in AERONET's algorithm, show good agreement in fine mode r_{eff} with AERONET's values shown in Figure 8 (being larger only by about 0.015 μm on average, and showing 55% correlation). This confirms that our differences with AERONET in aerosol size retrievals are primarily due to differences of approach to NO_2 absorption. *Gianelli* [2004] retrieved fine mode effective radii from RSS data that were also on average larger than those retrieved by AERONET and ascribed some of the differences to the omission of gaseous (NO_2 and water vapor) absorption in the short wavelength AERONET retrievals.

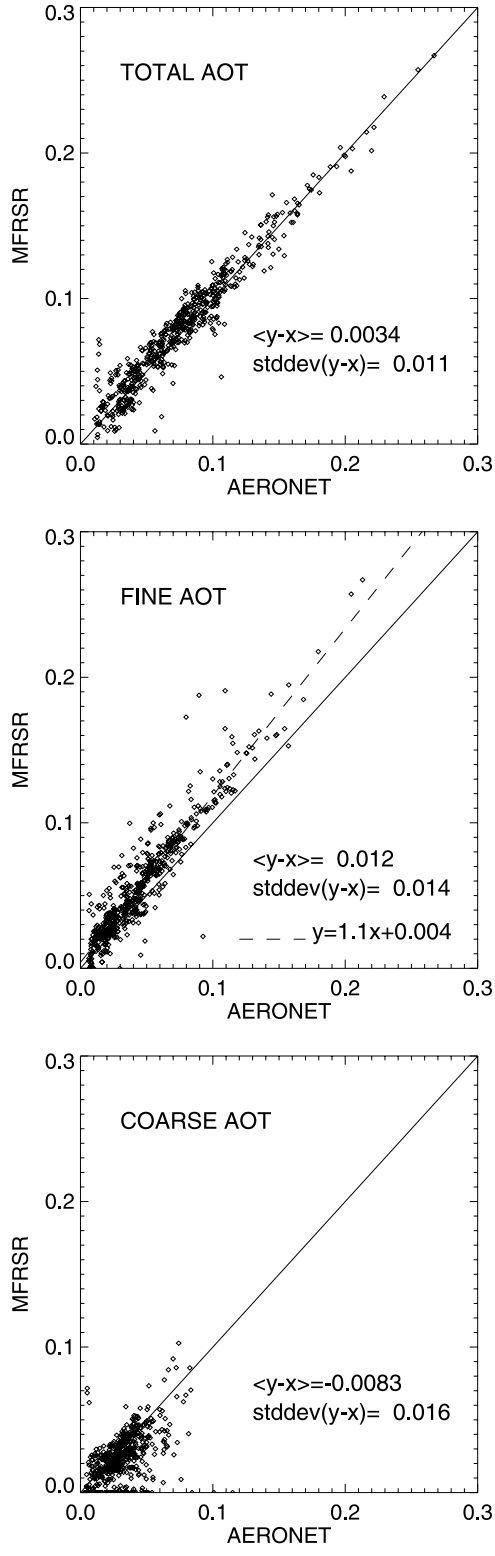

Figure 7. Comparison between MFRSR-derived AOTs at 870 nm wavelength (total, fine, and coarse) and those from AERONET almucantar scan analysis. The MFRSR (C1) and CIMEL sunphotometers are located at the SGP site Central Facility. The measurements from March 1998 to September 2000 were used (576 datapoints). The plots show that the presented mode separation method produces slightly higher values of fine mode AOT (and, correspondingly, lower values of coarse AOT) than the AERONET retrievals. The difference in fine AOT can be characterized either as 0.01 on average or as 10% of the AERONET values (the latter is shown by the dashed line).

[24] The effects of neglecting NO_2 absorption in the retrieval of aerosol size distributions were studied by *Schroeder and Davies* [1987], who analyzed simultaneous spectrometric and photometric measurements made at a suburban site in Canada that is significantly affected by industrial pollution. They measured up to 12 DU of column NO_2. Their inversions of aerosol size distributions made from sunphotometric data corrected for spectrometrically measured NO_2 show "fewer particles at radii smaller than 0.2 μm", indicating that the observed correspondence between high NO_2 values and larger aerosol particles may not be simply a retrieval artifact, since both larger nitrate aerosol particles and NO_2 come from the same NO_x emissions.

[25] We should emphasize, however, that due to the spectral trade-offs between NO_2 absorption and small particle extinction, actually separating their spectral signatures requires high measurement accuracy and higher spectral resolution. Some technical artifacts (e.g. inadequate knowledge of the instrument's spectral response, or poor calibration due to lack of clear days) can also affect the separation results. Thus, combining the results of unconstrained retrievals and those retrieved assuming zero NO_2 column amounts is a better alternative as it allows us to more accurately bracket the actual solution space. The shortcomings of both approaches would be eliminated if photometric data were complemented by high-resolution spectrometric measurements in 300–500 nm spectral range.

3.2. Detection of Mt. Pinatubo Volcanic Aerosols

[26] Data collected at the SGP CF for the time period 1993–97 provides a unique opportunity to study the decay of the stratospheric aerosol following the eruption of Mt.

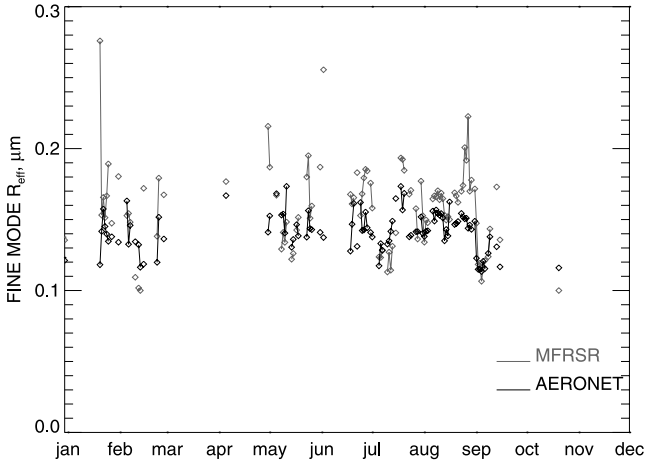

Figure 8. Time series of daily mean fine mode effective radii retrieved from AERONET almucantar measurements and from MFRSR data for the same days in 2000. MFRSR values are obtained under zero NO_2 constraint.

Pinatubo in June 1991. The decay of the Pinatubo aerosol has been well-documented by a variety of sun-photometric [*Michalsky et al.*, 2001], lidar [e.g., *Osborn et al.*, 1995], in situ [e.g., *Goodman et al.*, 1994], satellite [e.g., *McCormick and Veiga*, 1992], and combinational studies [e.g., *Russell et al.*, 1996]. The study by *Michalsky et al.* [2001] based on the analysis of MFRSR measurements obtained at the SGP site, as well as at two other sites in Pennsylvania and West Virginia, reported a decline in total optical thickness with a corresponding increase in the Angstrom exponent at all three locations during the 1992–95 time period. Our retrievals for this time period are shown in Figure 9. The Pinatubo aerosol tend to fall in the coarse mode and the AOT values decrease during 1993–95, exhibiting little seasonal variability. In contrast, the fine mode AOT values show no decreasing trend during this time period but do exhibit seasonal variability with AOT maxima in summer time. These results are in qualitative agreement with the 1991–1993 in situ measurements reported by *Goodman et al.* [1994] and *Russell et al.* [1996] demonstrating that in 1993 (2 years after the eruption) the size distribution of stratospheric aerosols had become essentially bimodal.

3.3. Sulfate and Nitrate Aerosols at SGP Site

[27] Analysis of a year (2000) of MFRSR data obtained at the SGP Extended Facilities reveals systematic geographical differences in the retrieved size of fine mode aerosols. The time series of the daily mean fine mode and monomodal r_{eff} retrievals for the year 2000 from the Central Facility (E13) and three Extended Facilities (E2, E4, and E24) are shown in Figure 4. As it is seen in Figure 5, E2 represents the northern part of SGP site, E4 – northwestern, E13 – central, and E24 – its southern part. These particular sites were chosen to represent three different aerosol size variability patterns characteristic of these different areas of the SGP. We identify these types of variability as A, B, and C. The respective areas dominated by these types are shown on the SGP site maps in Figure 17. Type A is characteristic of the North-East and South-West of the site and corresponds to larger 0.3–0.5 μm particles. Type C dominates the South-East and corresponds to very small aerosol particles with r_{eff} less than or equal to our detection limit 0.2 μm. Type B is intermediate between A and C and is encountered in the North-West and the central parts of the SGP where both very small and larger fine mode particles are present. The larger fine mode effective radii exhibit a seasonal maximum in winter. Attributing a data set to a particular type (A, B, or C) was done by visual analysis and is therefore subjective. For example, while we attribute the Central Facility (E13) data set to the C type it also has features consistent with type B. The annual mean particle effective radius might be a more quantitative determinate of type, however, at present we prefer to avoid averaging the actual retrievals with the detection limit values (0.2 μm) that are simply indicators of very small aerosol particles.

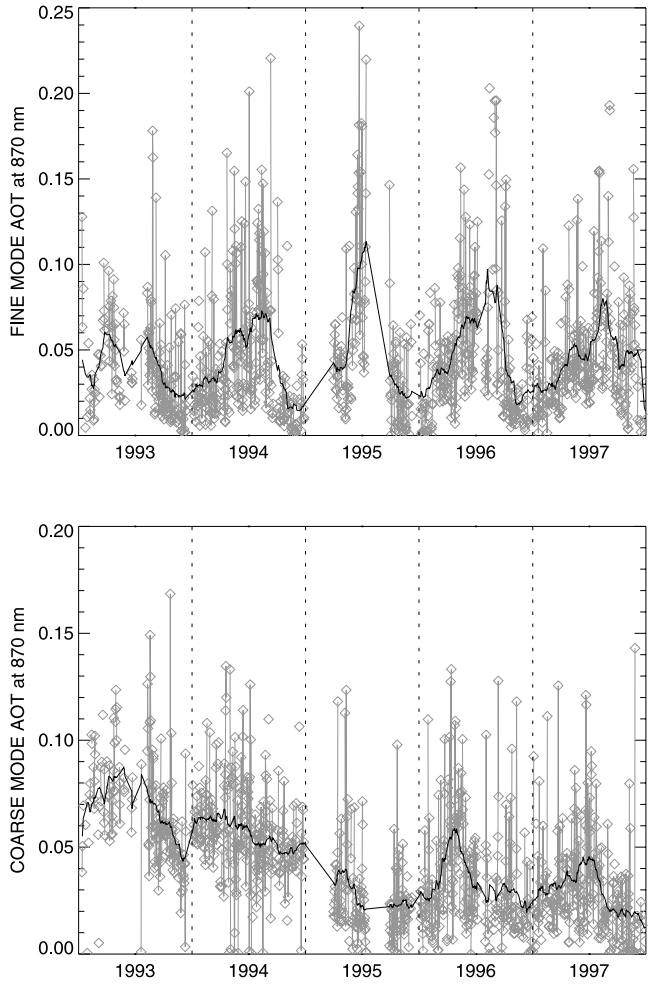

Figure 9. Time series of daily mean fine (top) and coarse (bottom) AOT retrieved from SGP Central Facility MFRSR data set for 1993–1997. The black curves show results of moving 3rd degree polynomial smoothing with 30 day window. The strong decreasing trend in the coarse AOT for the time period 1993–1995 corresponds to decay of stratospheric volcanic aerosols from the June 1991 Pinatubo eruption. Distinct from the coarse mode, the time series of fine mode AOT shows no inter-annual decrease while exhibiting a strong annual cycle with maxima in summer.

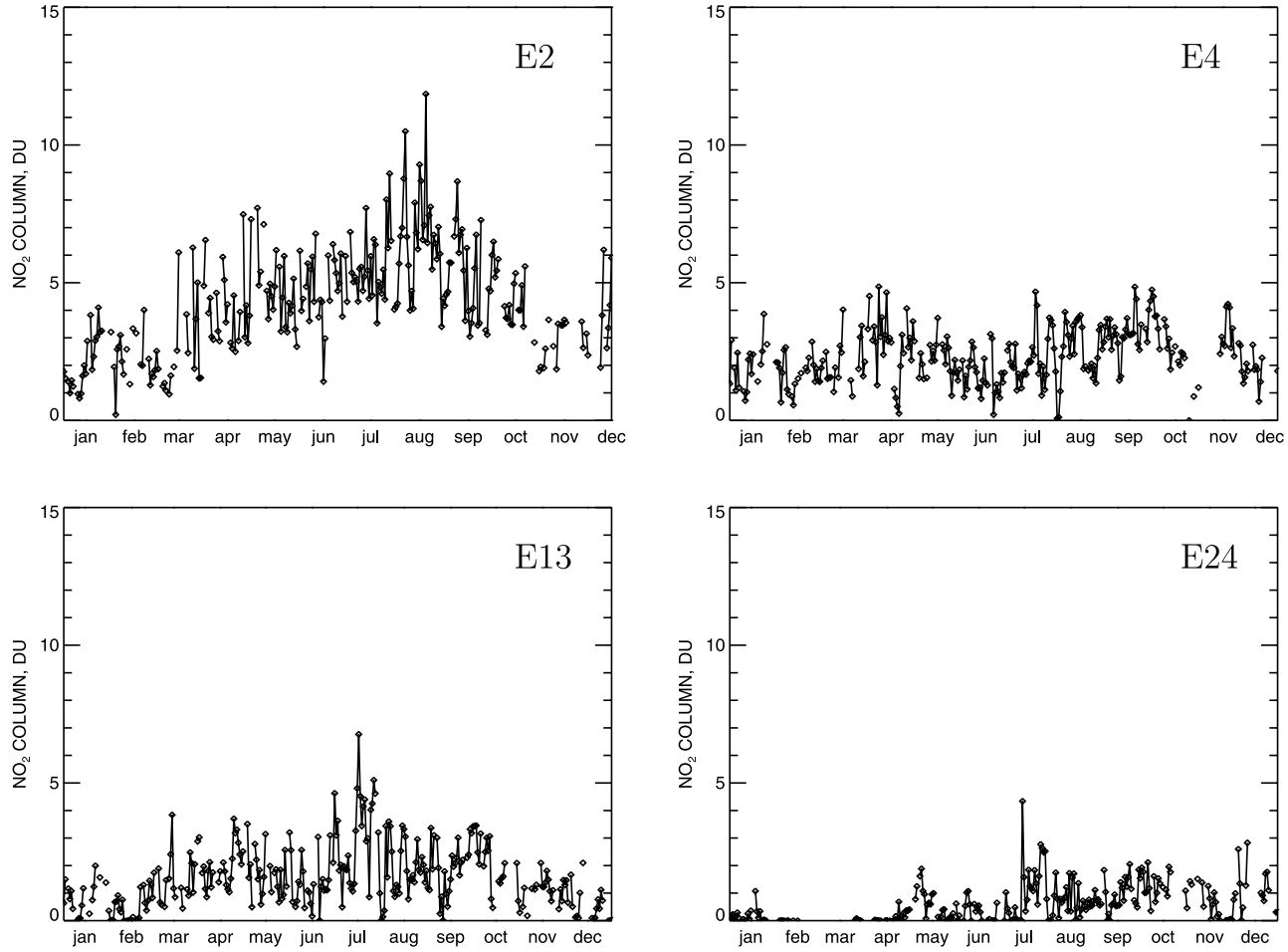

Figure 10. Time series of daily mean column amounts of NO_2 inferred for SGP Extended Facilities E2, E4, E13, and E24 for the year 2000. Small (less than 1 DU) negative amounts of NO_2 inferred for parts of E24 data set are set to zero.

[28] As discussed above, the values of r_{eff} obtained using the constrained variant of our algorithm with NO_2 amount set to zero are smaller for type A and B sites compared to type C sites. This may be a result of neglecting of relatively large NO_2 amounts (Figure 10) that may actually be present and coming from the same pollution sources as the aerosols. The amounts at E2 are particularly high (up to 10 DU on some days) however they do not exceed values reported for sites influenced by industrial pollution [*Schroeder and Davies*, 1987]. Amounts of NO_2 estimated by *Gianelli et al.* [2005] from differential absorption analysis of RSS data from SGP's Central Facility while being generally lower than MFRSR-derived values but are within the accuracy of the MFRSR retrievals (at best ±1 DU). Gaseous absorption being misinterpreted as a contribution from very small aerosol particles effectively decreases the retrieved size of fine mode aerosol. This decrease is complemented with an increase in the coarse mode fraction in AOT, so that the Angstrom exponent in the longwave spectral region outside NO_2 absorption band remains intact. The same trend is observed in Figure 7 comparing fine and coarse AOTs derived from MFRSR data with account to NO_2 with AERONET values obtained with zero NO_2 assumption. While NO_2 absorption is a main source of uncertainty in photometric retrievals of aerosol size, NO_2 column amounts are poorly constrained by photometric means. However, the quantitative differences between the sites described above can be seen directly from spectral dependence of measured optical thicknesses. Figure 11 shows plots of daily mean shortwave (415–500 nm) and longwave (550–870 nm) aerosol Angstrom exponents (for the sake of comparison the NO_2 contribution has not been removed from 415 and 500 nm channels, while NO_2 absorption at 550 and 870 nm is virtually zero). The differences between sites in longwave exponents are in agreement with those in fine mode size for unconstrained retrievals. The same can be more cautiously said about relation between shortwave exponents and aerosol sizes from zero-NO_2 results: the exponents from E2 are larger than those from E24, however the difference is less pronounced than for their longwave counterparts. The most important factor in our view distinguishing the four sites is the difference between short- and longwave exponents for each site. Indeed, while for E24 these exponents have very similar values, E2 data set shows a significant difference indicating a "break" in spectral dependence of optical thickness. This effect is also well-pronounced in the annual mean spectral optical thicknesses plots in Figure 12. Such a difference between spectral intervals one of which is

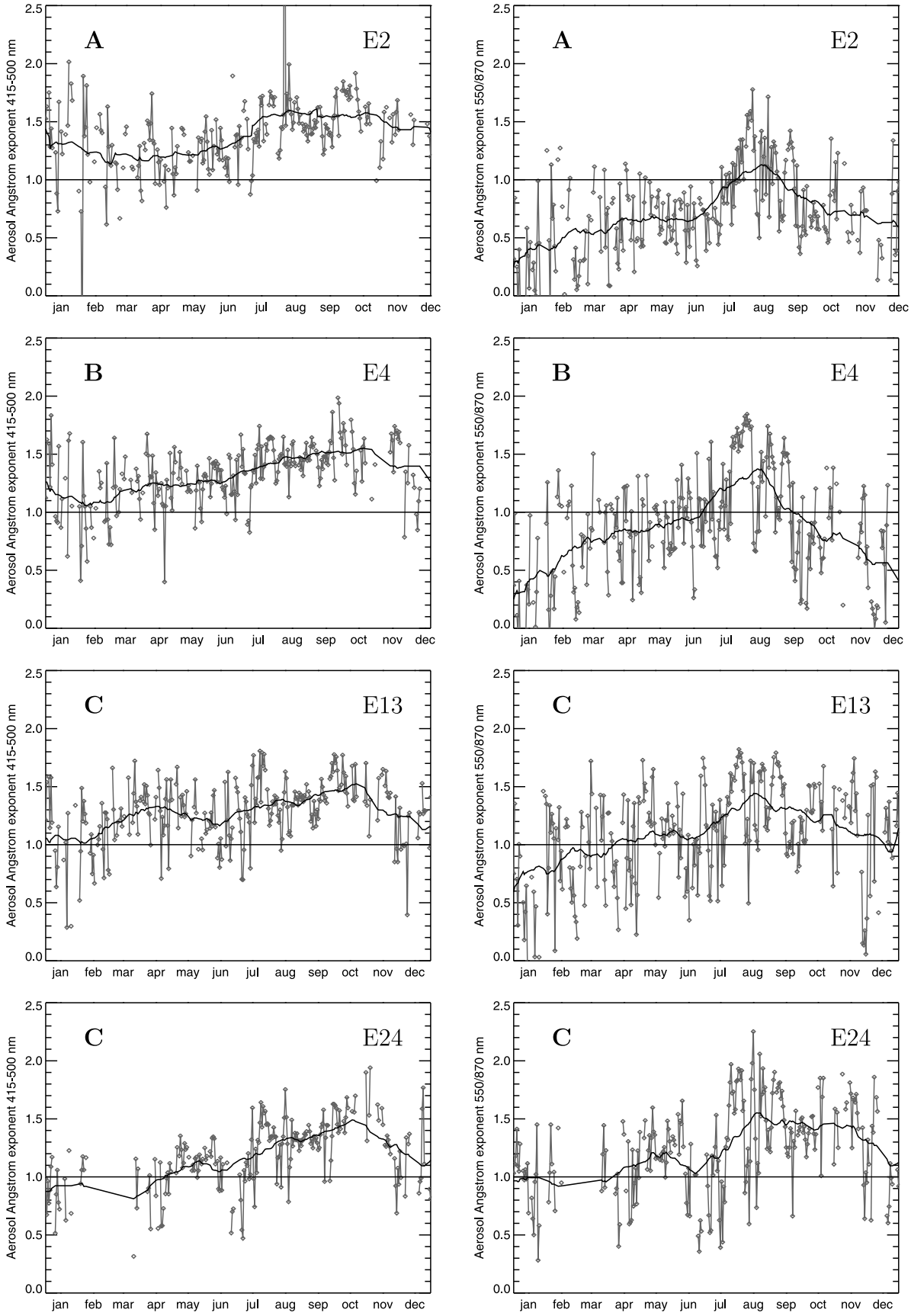

Figure 11. Time series of daily mean 415–500 nm (left) and 550–870 nm (right) Angstrom exponents for SGP Extended Facilities E2, E4, E13, and E24 for the year 2000. The value of 1 is shown by the horizontal line to enhance comparison.

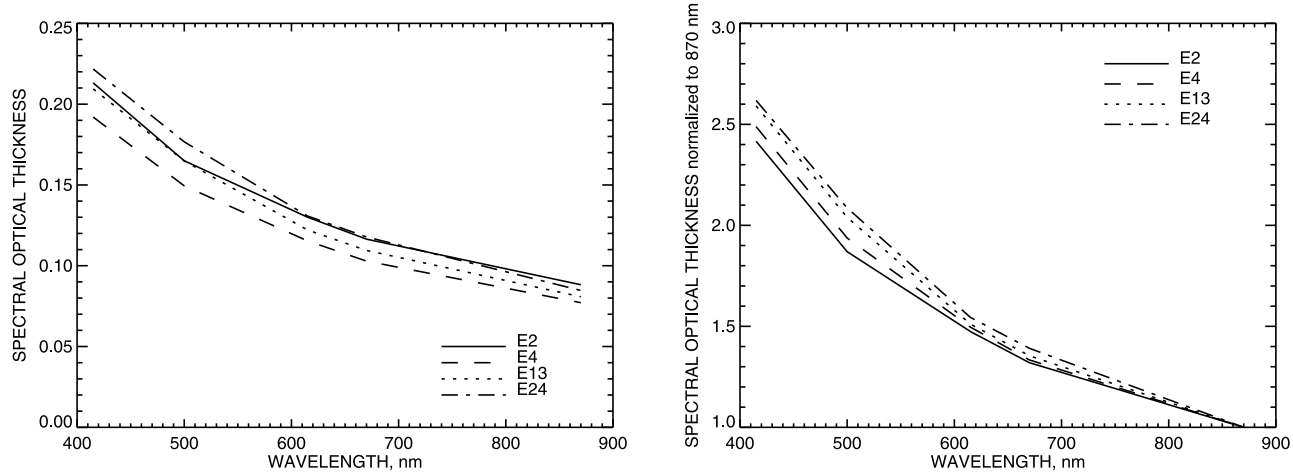

Figure 12. Annual mean total (with TOMS ozone subtracted) spectral optical thicknesses from SGP Extended Facilities E2, E4, E13, and E24 for the year 2000 (left). (right) The same spectral dependences normalized to unity at 870 nm wavelength to enhance spectral slope comparison.

affected by NO_2 absorption and the other is not is likely to be attributed to the presence of non-negligible NO_2 amounts, however we cannot rule out a sharply bimodal aerosol size distribution.

[29] The plots of daily mean total, fine, and coarse AOT (at 550 nm wavelength) from E2, E4, E13, and E24 are presented in Figure 13. In these plots the monomodal retrievals with $r_{\text{eff}} < 0.6$ μm are assigned to the fine mode, while those with $r_{\text{eff}} > 0.6$ μm are assigned to the coarse mode. These plots do not reveal any striking differences between these sites in terms of typical values or variability.

[30] We suggest that the above types of aerosol size variability may reflect a balance between different aerosol species at the SGP site, in particular, sulfates and nitrates. Aerosol sampling studies measuring size distributions of nitrate and sulfate particles have been performed in different environments, such as urban/industrial [*John et al.*, 1990; *Neusü et al.*, 2002; *Mallet et al.*, 2003; *Lestari et al.*, 2003; *Wittig et al.*, 2004], mountain [*Putaud et al.*, 2004], and marine [*Ottley and Harrison*, 1992] sites. All of these studies indicate that nitrate particles are generally larger than sulfates. Measurements by *John et al.* [1990] in southern California show that both sulfates and nitrates have tri-modal distributions with radii (half of aerodynamic diameter) of the modes being 0.1, 0.3–0.4, and 2 μm. However compared to sulfates, nitrates have larger second and third (supermicron) mode concentrations. The study by *Mallet et al.* [2003], performed in the industrial Marseille area in southern France, obtained generally monomodal (mass) size distributions for both species with maxima around a particle radius of 0.1 μm for sulfates, and 1–2 μm for nitrates. Other studies mentioned above also confirm, that compared to sulfates, nitrate aerosols have a notably larger concentration of particles with radii exceeding 0.6 μm in their cumulative size distributions. *Tang et al.* [1981] successfully used aerosol model with 0.1 μm (r_g of a log-normal size distribution) sulfate and substantially larger 0.3 μm nitrate modes to explain the observed relationship between atmospheric visibility and relative humidity.

[31] To further analyze the relationship between aerosol size and composition we considered sampling measurements performed directly at the SGP's Central Facility by NOAA Pacific Marine Environmental Laboratory (PMEL, http://saga.pmel.noaa.gov) (see *Quinn et al.* [2000] for a study based on PMEL measurements). Figure 14 shows time series of NO_3 and SO_4 ion mass concentrations in submicron (daily measurements) and supermicron (1–10 μm, weekly measurements) particulate matter measured by PMEL at SGP during the year 2000. Figure 15 presents ratios between the nitrate and sulfate concentrations in sub- and supermicron modes from Figure 14. The plots show that while the supermicron concentrations of nitrates and sulfates are comparable (the annual averages are 0.2 μg/m^3 for nitrates and 0.16 μg/m^3 for sulfates), sulfates strongly dominate the submicron mode: their annual average submicron concentration is 2.4 μg/m^3, that is an order of magnitude larger than the nitrate value of 0.14 μg/m^3. While this may indicate a stronger relative input of supermicron particles to the nitrate particle size distribution, compared to sulfate aerosol, these measurements present only simplified (2-point) proxies of the actual aerosol size distributions. Using them for estimation of relative size of submicron nitrate and sulfate particles requires an assumption that the observed trends (increase of nitrate concentrations with particle size opposite to the decrease of the sulfate concentrations) can be extended to the submicron size range, meaning larger size of submicron nitrate particles compared to sulfates. This means that the actual distribution shapes should be assumed to be sufficiently monotonic, rather than consisting of independent narrow modes.

Figure 13. Time series of daily mean aerosol optical thicknesses (at 550 nm) for the four measurement sites from Figure 4. Top plots represent the total AOT, middle plots represent the fine mode AOT, and bottom plots represent the coarse mode AOT. The monomodal retrievals with $r_{\text{eff}} < 0.6$ μm has been assigned to the fine mode, while those with $r_{\text{eff}} > 0.6$ μm - to the coarse mode.

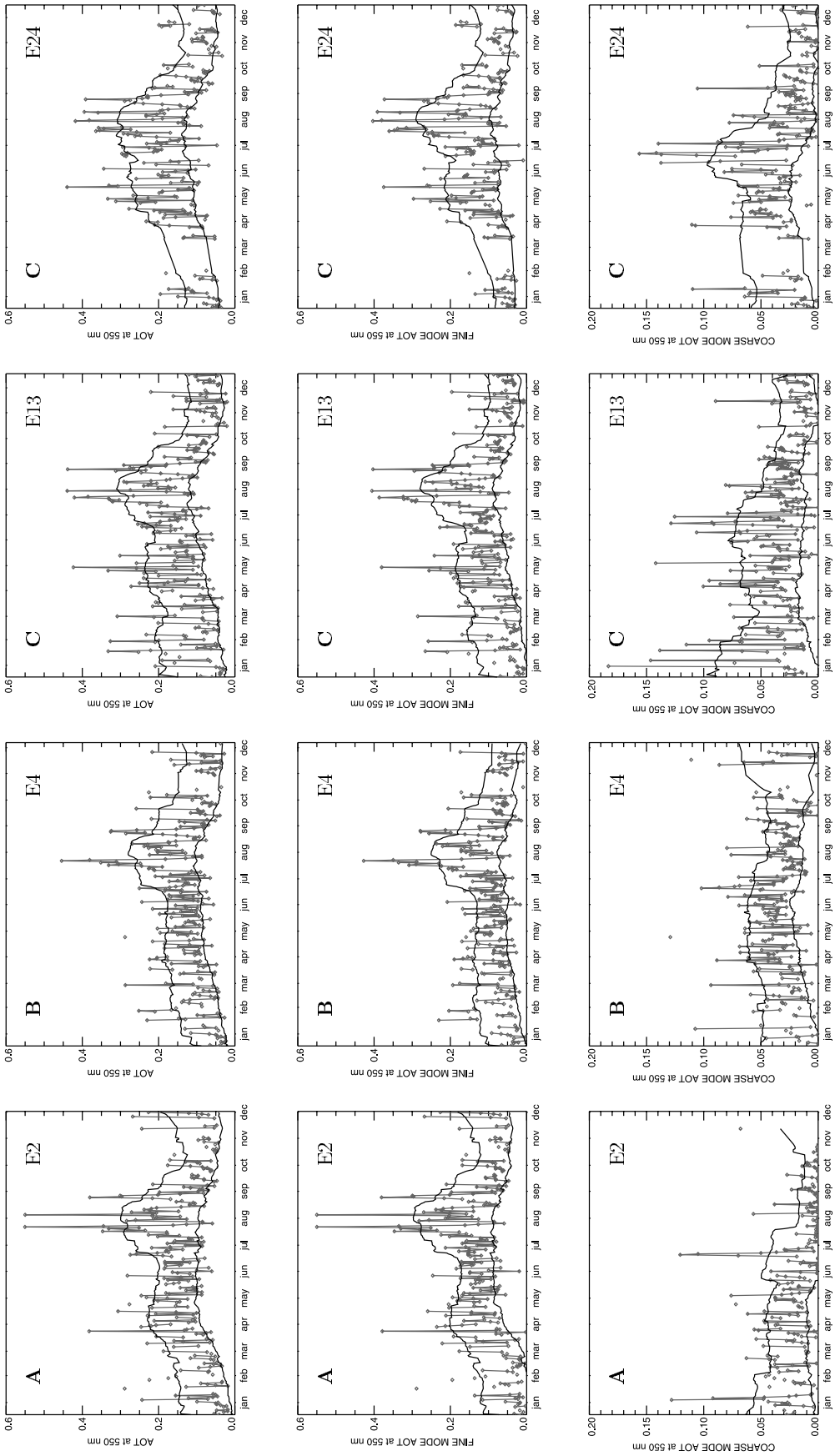
A
B
C
E2
E4
E13
E24
AOT at 550 nm
FINE MODE AOT at 550 nm
COARSE MODE AOT at 550 nm
0.0
0.2
0.4
0.6
0.00
0.05
0.10
0.15
0.20
jan feb mar apr may jun jul aug sep oct nov dec

Figure 13

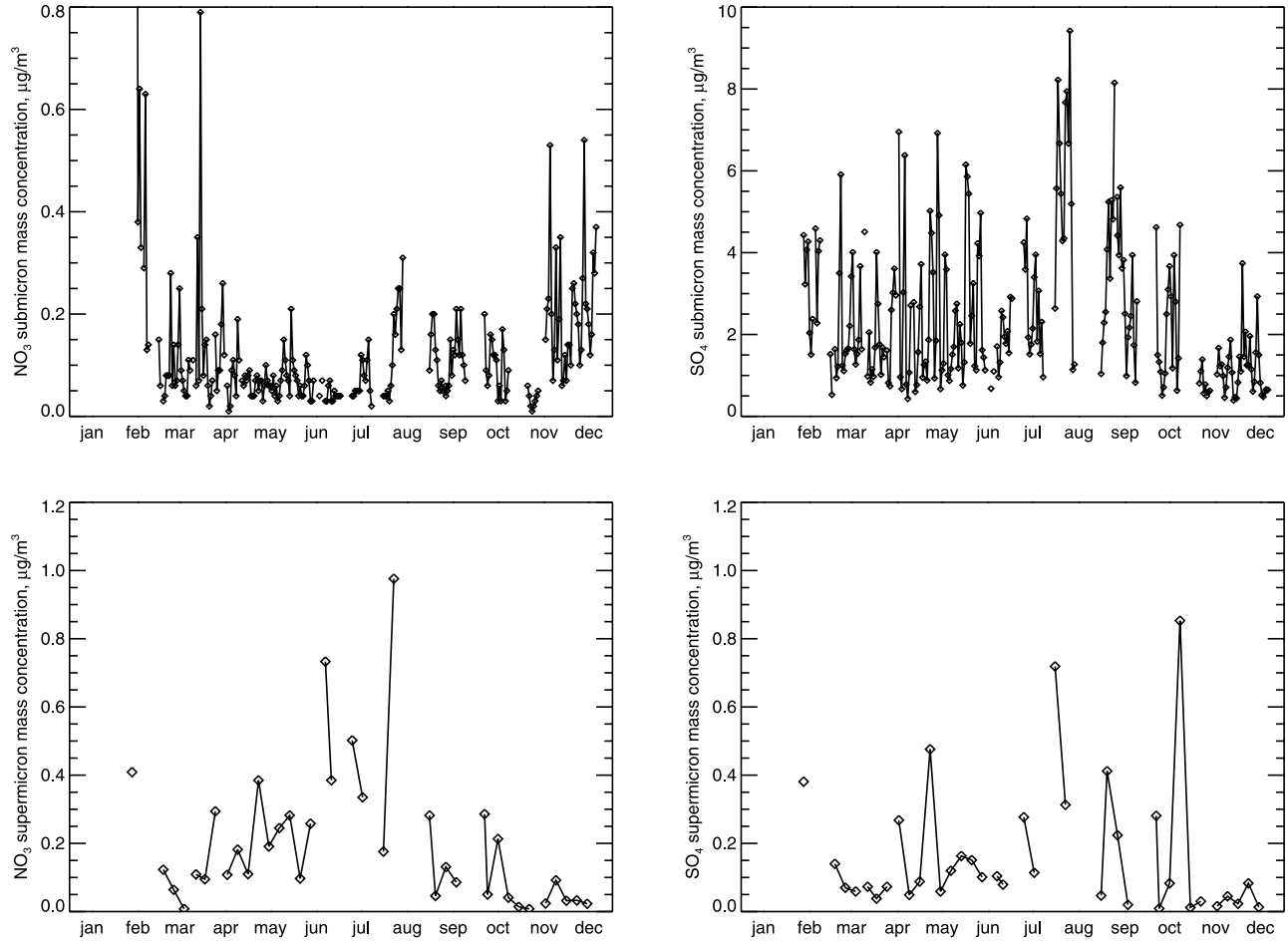

Figure 14. NO_3 (left) and SO_4 (right) ion mass concentrations in submicron (top) and supermicron (1–10 μm, bottom) particulate matter measured in the year 2000 at SGP Central Facility by NOAA Pacific Marine Environmental Lab (PMEL).

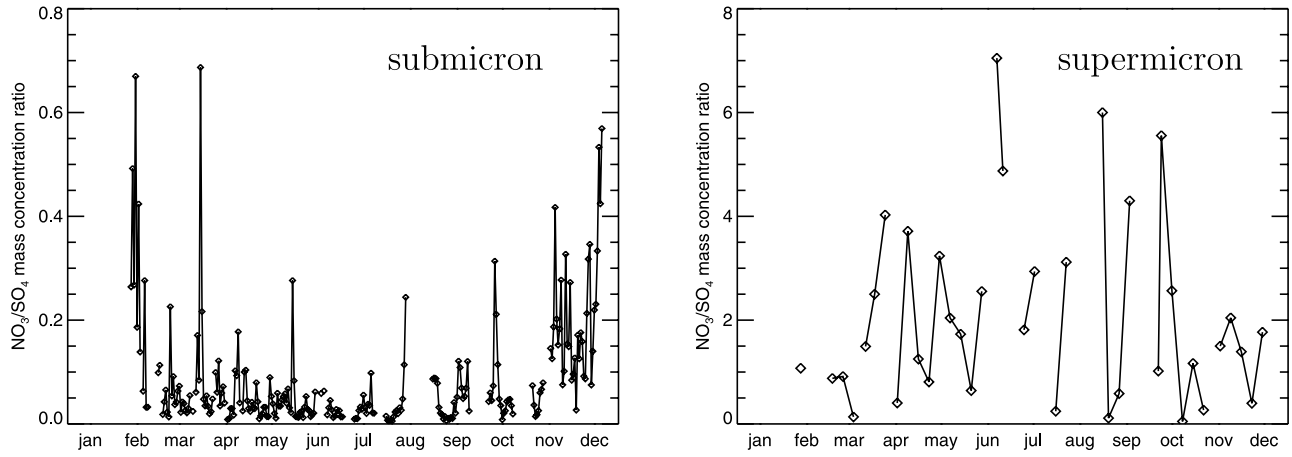

Figure 15. Ratios of NO_3/SO_4 ion mass concentrations from Figure 14 in (left) submicron and (right) supermicron particulate matter. The plots show that the submicron fraction is dominated by sulfate particles, while nitrate particles constitute a larger part of the supermicron fraction. This fact reflects a difference in particle size distributions between the two species with nitrate particles being generally larger. The annual cycle variations in fine mode ratios are attributable to those in nitrate and sulfate concentrations having maxima in winter and summer, respectively.

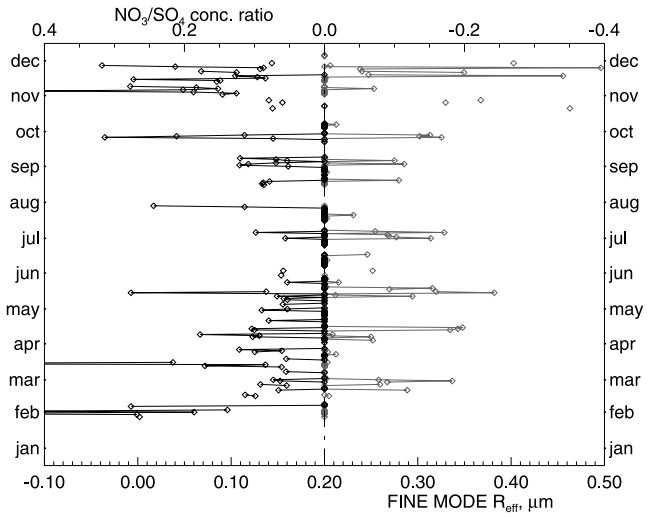

Figure 16. Comparison between the fine mode nitrate/sulfate ratios (left) from Figure 15 and the fine mode effective radius time series (right) for E13 site from Figure 4 (left bottom panel). The NO_3/SO_4 ratios less than 0.05 are set to zero to reflect the lower limit of 0.2 μm in our retrievals of r_{eff}. During the year 2000 there were 188 days when both measurements were available. Out of this number, for 29 days larger r_{eff} (>0.2 μm) corresponded to larger (>0.05) nitrate/sulfate ratio, for 86 days both quantities were small. These two numbers together constitute 61.2% of the total number of cases. The total number of days with $r_{eff} > 0.2$ were 45, 29 of them with nitrate/sulfate ratio exceeding 0.05 constitute 64.4%, i.e. almost 2/3.

[32] Figure 14 also reveals seasonal cycles in submicron aerosol concentrations with a maximum in winter for nitrates, and in summer for sulfates. Similar seasonal variability has been reported by *Wittig et al.* [2004] for a different site (Pittsburgh, Pennsylvania). The resulting seasonal trend in NO_3/SO_4 ratios (Figure 15, left) has certain resemblance to that in our retrievals of fine mode r_{eff} for SGP's Central Facility (E13, Figure 4). It appears that this resemblance goes beyond just seasonal means, but is often present in day-to-day changes in the concentration ratio as reflected in the corresponding changes in the retrieved effective radius. We illustrate this in a "butterfly" plot (Figure 16) comparing the two quantities for days when both are available. In this plot we set the NO_3/SO_4 ratios less than 0.05 to zero to reflect the absence of variability in our r_{eff} values below the retrieval limit of 0.2 μm. The plot shows a certain degree of correspondence between the two data sets: among the total of 188 daily values, in 29 cases we have $r_{eff} > 0.2$ μm while the NO_3/SO_4 ratio exceeds 0.05, and in 86 days both quantities were smaller than their corresponding limit values. These two numbers together constitute 61% of the total number of cases. The fraction of the cases supporting the above correspondence is even higher for the period from June to December.

[33] Given the high concentrations of sulfates compared to nitrates in the submicron mode, it is expected that the sulfate contribution will dominate both the fine mode and total AOT which, as shown in Figure 13, have maxima in summer when submicron sulfate concentrations are the highest. Analysis of multi-year PMEL data sets from the SGP and other continental US sites indicates that supermicron concentrations of sulfates and nitrates do not exhibit an annual cycle. The summer maximum in nitrate concentrations in Figure 14 is found to be specific to this particular year and site. However, we should note a similarity between the time dependence of these concentrations and those of coarse mode AOT presented in Figure 13 for E13.

[34] To investigate a possible relationship between geographical differences in retrieved aerosol fine mode r_{eff} and the spatial variations in aerosol composition we used the NO_3/SO_4 ion concentration ratios obtained from National Atmospheric Deposition Program/National Trends Network (NADP/NTN, http://nadp.sws.uiuc.edu) precipitation monitoring sites in Oklahoma, Kansas and all of the states having a common border with these two. The result of interpolation between the mean values for the year 2000 is shown as a contour plot in Figure 17 (left). This plot shows a trend corresponding to domination of nitrates in A-zones (especially in the North) as opposed to domination of sulfates in the C-zone in the South-East of the SGP site. The observed geographical trends in the fine mode aerosol particle size are also in agreement with the ratios between PM2.5 and PM10 sampling measurements from EPA AirData (http://www.epa.gov/air/data/) monitoring stations in Oklahoma, Kansas, and surrounding states (Figure 17, right). Despite the fact that our fine mode particles are small enough to contribute equally to both PM2.5 and PM10, such a comparison still makes sense, since, as discussed above, the difference between sulfate and nitrate aerosols is observed over the whole size range. In other words, our photometric measurements detect the small-size signature of this difference, while the sampling data reflects its manifestation on a broader particle size scale. EPA AirData reports also indicate that among power plants in the area surrounding the SGP site these located in north-eastern Kansas (i.e. in the area where we retrieve larger aerosol sizes) have the largest ratio of NO_x to SO_2 emissions.

4. Conclusions

[35] A new improved version of the MFRSR retrieval algorithm of *Alexandrov et al.* [2002] is presented. The new version is capable of separating fine and coarse mode AOT, as well as retrieving a quantitative measure of the fine mode effective radius. The coarse mode effective radius is assumed to be fixed. The new algorithm can also perform retrievals with a monomodal size distribution (determining total AOT and effective radius) when the coarse mode is absent or when the fine mode size becomes too large to make fine and coarse mode extinction indistinguishable in the visible spectral range. In the cases when the fine mode size is smaller than 0.2 μm, the retrievals of fine and coarse AOT are performed with both fine and coarse particle sizes fixed. As in the earlier algorithm, column amounts of ozone and nitrogen dioxide are also retrieved, and the instrument calibration constants are determined from the data. These retrievals are complemented with those made under zero NO_2 assumption to provide lower limit of the solution space for fine mode effective radius, that is particularly valuable in

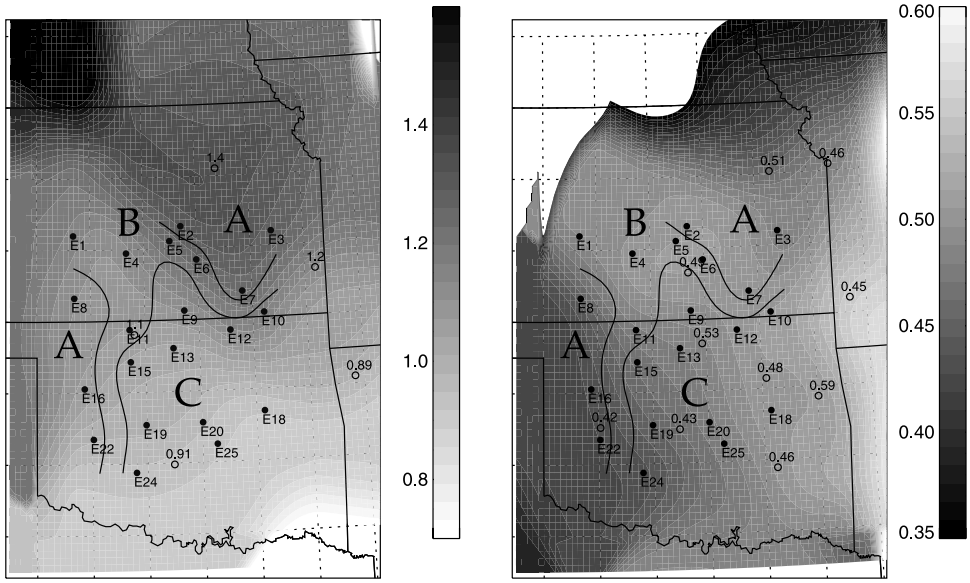

Figure 17. (left) Contour plot of the NO_3/SO_4 ion concentration ratios (mean values for the year 2000) obtained from National Atmospheric Deposition Program/National Trends Network (NADP/NTN) precipitation monitoring sites. (right) Contour plot of the PM2.5 to PM10 ratios (mean values for the year 2000) obtained from EPA AirData monitoring sites. In both plots sampling sites in Oklahoma, Kansas and all states with common border with these two were used to construct the contour plots. Total of 13 NADP sites and 40 EPA sites were used. The sampling sites in SGP vicinity are shown by open circles with the corresponding values. Discrimination between aerosol types A, B, and C has been made by visual examination of fine mode effective radius time series similar to those in Figure 4. The geographic areas corresponding to these types are separated by (artificial) black curves. In both plots the types A and B of aerosol fine particles appear to correspond to nitrate-dominated (small PM-ratio) areas, while the smaller particles (type C) are encountered in the sulfate-dominated (high PM-ratio) South-East of the SGP site. The MFRSR instrument locations are shown by solid circles.

the cases when unconstrained retrievals show the fine mode size smaller than 0.2 μm. Since the unconstrained retrievals in these cases are performed with assumed maximal fine mode r_{eff} = 0.2 μm, the retrieved NO_2 amounts provide the upper bounds for the actual values.

[36] The retrievals made with the new algorithm using the extensive DOE ARM program CART site multi-instrument data set are compared with aerosol measurements made using other instruments and analysis techniques. In particular, our comparison with AERONET almucantar retrievals reveals statistically similar total AOT estimates, but our algorithm produced a 10% larger fine mode AOT and correspondingly smaller coarse mode AOT. This difference arises from differences in the fine mode aerosol effective radius that is consistently lower in AERONET retrievals than our default minimal value of 0.2 μm. Since setting the NO_2 column amount to zero (as is assumed in AERONET retrievals) produces the smallest possible fine mode effective radius we included a solution obtained under zero NO_2 assumption. Not surprisingly, the results are in much closer agreement with AERONET retrievals both in fine mode r_{eff} values and mode separation. This suggests that the difference in retrieval approach in dealing with NO_2 absorption is the main reason for disagreement between the two data sets. The fact that omission of NO_2 and water vapor absorption at 440 nm in the AERONET almucantar retrievals may lead to underestimation of the fine mode r_{eff} has been also noted by *Gianelli* [2004].

[37] The retrievals performed on the 1993–97 data set from the SGP Central Facility shows that our algorithm correctly interprets the multi-year decrease in AOT and increase in Angstrom parameter during 1993–95 to the dissipation of coarse mode particles introduced in the stratosphere by the 1991 eruption of Mt. Pinatubo. The time series of fine mode effective radius retrieved from the data obtained at the SGP Extended Facilities during the year 2000 appear to reflect geographic and temporal changes in the balance between sulfate and nitrate aerosol fractions (the latter having larger size particles). The difference between fine mode particle sizes retrieved with standard (unconstrained) and constrained (zero NO_2) is substantially larger in the areas with substantial NO_x emissions, which may suggest that both nitrate aerosols and NO_2 have NO_x as their precursor.

[38] The unconstrained algorithm is less stable than its constrained counterpart and does not allow the retrieval of fine mode aerosol r_{eff} values smaller than 0.2 μm. The estimated accuracy of our NO_2 retrievals is not better than 1–2 DU. On the other hand, a solution predicated on assumed NO_2 column amounts is not justified in light of work of *Schroeder and Davies* [1987]. However, constrained retrievals using reasonable climatological estimates of minimal NO_2 amounts (e.g. stratospheric amounts or even zero) can improve retrievals of aerosol properties by providing minimal physically allowed fine mode size and fine mode fraction in AOT. We believe that the only way to

produce aerosol retrievals that would not be biased by the treatment of NO_2 is to complement photometric (CIMEL or MFRSR) data with high spectral resolution measurements that allow differential absorption techniques to be used for NO_2 retrievals. Such measurements would be particularly useful if made at the photometers locations, however climatological estimates would be also helpful.

[39] All of the data processing steps required in the algorithm are fully automated. The algorithm performs the cloud screening, calibration and retrieval steps as well as saves the retrieval results in netCDF ARM-style format. Our future plans include detailed sensitivity study and error analysis of the presented retrieval algorithm. We will also continue our work on creation of an aerosol climatology from the analysis of multi-year multi-instrument data sets available from the SGP as well as sites operated by other MFRSR networks.

[40] **Acknowledgments.** We would like to thank M. J. Bartholomew for her effort in maintaining the AERONET site at SGP. The authors acknowledge the availability on the web of the National Atmospheric Deposition Program/National Trends (NADP/NTN, http://nadp.sws.uiuc.edu) precipitation monitoring data set as well as NOAA Pacific Marine Environmental Laboratory (PMEL, http://saga.pmel.noaa.gov) and EPA AirData (http://www.epa.gov/air/data/) aerosol sampling data sets. We are indebted to both reviewers of this paper for the deep and thoughtful comments that significantly contributed to substantial improvement of this paper. This research was supported by the Atmospheric Radiation Measurement (ARM) Program sponsored by the U.S. Department of Energy, Office of Science, Office of Biological and Environmental Research, Environmental Sciences Division (interagency agreements DE-AI02-93ER61744 and DE-AI02-95ER61961), and by NASA's Radiation Science Program (RTOP 622-46-05-30).

References

Alexandrov, M. D., A. Lacis, B. Carlson, and B. Cairns (2002), Remote sensing of atmospheric aerosols and trace gases by means of Multi-Filter Rotating Shadowband Radiometer. part I: Retrieval algorithm, *J. Atmos. Sci.*, *59*, 524–543.

Alexandrov, M. D., A. Marshak, B. Cairns, A. A. Lacis, and B. E. Carlson (2004a), Automated cloud screening algorithm for MFRSR data, *Geophys. Res. Lett.*, *31*, L04118, doi:10.1029/2003GL019105.

Alexandrov, M. D., A. Marshak, B. Cairns, A. Lacis, and B. Carlson (2004b), Scaling properties of aerosol optical thickness fields retrieved from ground-based and satellite measurements, *J. Atmos. Sci.*, *61*, 1024–1039.

Dubovik, O., and M. D. King (2000), A flexible inversion algorithm for retrieval of aerosol optical properties from Sun and sky radiance measurements, *J. Geophys. Res.*, *105*, 20,673–20,696.

Dubovik, O., B. Holben, T. F. Eck, A. Smirnov, Y. J. Kaufman, M. D. King, D. Tanre, and I. Slutsker (2002), Variability of absorption and optical properties of key aerosol types observed in worldwide locations, *J. Atmos. Sci.*, *59*, 590–608.

Franssens, G., M. De Maziere, and D. Fonteyn (2000), Determination of the aerosol size distribution by analytic inversion of the extinction spectrum in the complex anomalous diffraction approximation, *Appl. Opt.*, *39*, 4214–4231.

Gianelli, S. M. (2004), Retrieving aerosols, ozone, and NO_2 using MFRSR, RSS, and CIMEL data, Ph.D. thesis, 244 pp., Columbia Univ., New York.

Gianelli, S. M., B. E. Carlson, and A. A. Lacis (2005), Aerosol retrievals using rotating shadowband spectroradiometer data, *J. Geophys. Res.*, *110*, D05203, doi:10.1029/2004JD005329.

Goodman, J., K. G. Snetsinger, R. F. Pueschel, G. V. Ferry, and S. Verma (1994), Evolution of Pinatubo aerosol near 19 km altitude over western North America, *Geophys. Res. Lett.*, *21*, 1129–1132.

Hansen, J. E., and L. D. Travis (1974), Light scattering in planetary atmospheres, *Space Sci. Rev.*, *16*, 527–610.

John, W., S. M. Wall, J. L. Ondo, and W. Winklmayr (1990), Modes in the size distributions of atmospheric inorganic aerosol, *Atmos. Environ., Part A*, *24*, 2349–2359.

Lestari, P., A. K. Oskouie, and K. E. Noll (2003), Size distribution and dry deposition of particulate mass, sulfate and nitrate in an urban area, *Atmos. Environ.*, *37*, 2507–2516.

Li, J., J. G. D. Wong, J. S. Dobbie, and P. Chylek (2001), Parameterization of the optical properties of sulfate aerosols, *J. Atmos. Sci.*, *58*, 193–209.

Mallet, M., J. C. Roger, S. Despiau, O. Dubovik, and J. P. Putaud (2003), Microphysical and optical properties of aerosol particles in urban zone during ESCOMPTE, *Atmos. Res.*, *69*, 73–97.

McCormick, M. P., and R. E. Veiga (1992), SAGE II measurements of early Pinatubo aerosols, *Geophys. Res. Lett.*, *19*, 155–158.

Michalsky, J. J., J. A. Schlemmer, W. E. Berkheiser, J. L. Berndt, L. C. Harrison, N. S. Laulainen, N. R. Larson, and J. C. Barnard (2001), Multiyear measurements of aerosol optical depth in the Atmospheric Radiation Measurement and Quantitative Links programs, *J. Geophys. Res.*, *106*, 12,099–12,107.

Neusüß, C., H. Wex, W. Birmili, A. Wiedensohler, C. Koziar, B. Busch, E. Brüggemann, T. Gnauk, M. Ebert, and D. S. Covert (2002), Characterization and parameterization of atmospheric particle number-, mass-, and chemical-size distributions in central Europe during LACE 98 and MINT, *J. Geophys. Res.*, *107*(D21), 8127, doi:10.1029/2001JD000514.

O'Neill, N. T., T. F. Eck, A. Smirnov, B. N. Holben, and S. Thulasiraman (2003), Spectral discrimination of coarse and fine mode optical depth, *J. Geophys. Res.*, *108*(D17), 4559, doi:10.1029/2002JD002975.

Osborn, M. T., R. J. DeCoursey, C. R. Trepte, D. M. Winker, and D. C. Woods (1995), Evolution of the Pinatubo volcanic cloud over Hampton, Virginia, *Geophys. Res. Lett.*, *22*, 3783–3797.

Ottley, C. J., and R. M. Harrison (1992), The spatial distribution and particle size of some inorganic nitrogen, sulfur and chlorine species over the North sea, *Atmos. Environ., Part A*, *26*, 1689–1699.

Putaud, J. P., R. Van Dingenen, A. Dell'Acqua, F. Raes, E. Matta, S. Decesari, M. C. Facchini, and S. Fuzzi (2004), *Atmos. Chem. Phys.*, *4*, 889–902.

Quinn, P. K., et al. (2000), Surface submicron aerosol chemical composition: What fraction is not sulfate?, *J. Geophys. Res.*, *105*, 6785–6805.

Russell, P. B., et al. (1996), Global to microscale evolution of the Pinatubo volcanic aerosol derived from diverse measurements and analyses, *J. Geophys. Res.*, *101*, 18,745–18,763.

Schroeder, R., and J. A. Davies (1987), Significance of nitrogen dioxide absorption in estimating aerosol optical depth and size distributions, *Atmos. Ocean*, *25*, 107–114.

Tang, I. N., W. T. Wong, and H. R. Munkelwits (1981), The relative importance of atmospheric sulfates and nitrates in visibility reduction, *Atmos. Environ.*, *15*, 2463–2471.

van de Hulst, H. C. (1981), *Light Scattering by Small Particles*, Dover, Mineola, N. Y.

Wittig, A. E., N. Anderson, A. Y. Khlystov, S. N. Pandis, C. Davidson, and A. L. Robinson (2004), Pittsburgh air quality study overview, *Atmos. Environ.*, *38*, 3107–3125.

M. D. Alexandrov, B. Cairns, B. E. Carlson, and A. A. Lacis, NASA Goddard Institute for Space Studies, New York, NY 10025, USA. (malexandrov@giss.nasa.gov)